SOME STUDIES TOWARDS GENERALIZATION OF MESH PATTERN IN LOWER BOUND SOLUTION OF BEARING CAPACITY PROBLEMS

A Thesis Submitted in Partial
Fulfilment of the Requirements
for the Degree of
Master of Technology
by

Subrata Roy

Department of Civil Engineering
INDIAN INSTITUTE OF TECHNOLOGY KANPUR

April, 1996

CERTIFICATE

It is certified that the work contained in the thesis entitled *Some studies towards generalization of mesh pattern in lower bound solution of bearing capacity problem* by **Subrata Roy**, has been carried out under my supervision and that this work has not been submitted elsewhere for a degree.

P Basudhar
17.4.96

Dr. P.K. Basudhar
Professor
Department of civil Engineering
Indian Institute of Technology, Kanpur

APRIL 1996

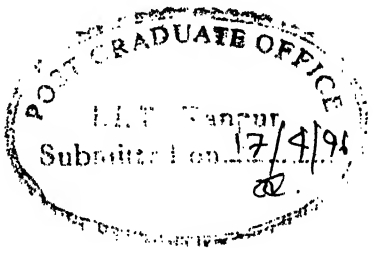

Abstract

The primary objective of this thesis is to develop a generalized mesh pattern for computing lower bound bearing capacity of foundations using the modified Lysmer's approach (Lysmer-Basudhar), for both homogeneous as well as layered soil profiles. In case of strip footings resting on homogeneous soil profile, a generalized mesh pattern has been developed. For strip footings resting on both vertically as well as horizontally stratified soil deposits a fair amount of success in generating the generalized mesh pattern has been achieved. The lower bound solutions predicted by these mesh patterns have been found to be in close agreement with other reported solutions. The obtained stress fields have been found to be extensible indicating that these are the true lower bound solutions.

ACKNOWLEDGEMENTS

To the utmost depth of my heart, I cannot visualize the epitomizing of my thesis work without the help of some of my nears and dears.

First and the foremost, I would like to express my deep gratitude and appreciation to Professor P.K.Basudhar for his inspiring guidance and arduous supervision, which were instrumental in the completion of this work. He provided me with necessary flexibility and freedom to work, a feature of his guidance, albeit keeping a watchful eye on the progress. I sincerely cherish his words of encouragements and counsel.

A special word of appreciation is due to all the faculties of civil engineering department under whose able guidance I could gain a knowledge of this field. I owe heartfelt gratitude towards all of my caring friends, without mentioning their names, who have in all possible ways extended their help as and when needed.

SUBRATA ROY

Contents

LIST OF TABLES

LIST OF FIGURES

NOTATIONS

a_j = Coefficient to σ_j in linear function to be optimized.

a_{ij} = Coefficient to σ_j in linear constraint number i.

$[A]$ = Coefficient matrix of the linear equality constraints.

b_i, b = Coefficients.

B = Width of footing.

$[B]$ = 9x7 matrix, geometrical property of the element.

C_u = Undrained cohesive strength of the soil.

C = Cohesion of the soil.

$\{\mathrm{D}\}$ = Design vector.

$\mathbf{D_m}$ = Optimum design vector.

δ = Angle of surface friction.

δ_t = Transition term between two types of penalty terms.

$F(\mathrm{D})$ = Objective function.

$[G]$ = 9x7 matrix, geometrical property of the element.

$\{g\}$ = 9 component vector related to body forces inn_{th} element.

g_j = Inequality constraints.

H = Depth of the top layer of soil deposit.

$\{h\}$ = 9 component vector related to body forces inn_{th} element.

M = Total number of inequality constraints.

m, n = Element numbers.

r_k = Penalty parameter.

$[S]$ = 7x9 matrix, geometrical property of n_{th} element.

$\{\bar{s}_i\}$ = 3 component internal stress vector at node i of element n.

s = 9 component stress vector which defines internal stresses in n_{th} element.

$[T]$ = 6x9 matrix, geometrical property of n_{th} element.

= x coordinate of nodal point i.

= z coordinate of nodal point j.

γ_z = Body forces per unit volume in x and z directions.

= Slope of element side connecting nodal points i and j.

$,\epsilon$ = Known coefficients.

$_i$ = Normal stress on vertical plane through nodal point i.

$_i$ = Normal stress on horizontal plane through nodal point i.

= Normal stress at nodal point i on plane parallel to element side jk of element n.

$_j$ = Normal stress at point i of element n on side ij.

= Stress vector which defines the complete stress field.

^{n} = 7 component stress vector which defines external normal stress on n_{th} element.

$_{zx,i}$ = Shear stress on horizontal plane at nodal point i.

$_{i,j}$ = Shear stress at node i on the side connecting points i andj.

$\cdot^n$ = 6 component stress vector which defines the external shear stresses on $\dot{n}_{th}$ element.

ϕ = Angle of internal friction.

Chapter 1

Introduction

The problems of soil mechanics are generally categorized into two distinct groups namely stability problems and elasticity problems. In stability problems the condition of ultimate failure of the soil mass is considered and the critical load causing such failure is determined. In contrast in elasticity problems the stresses and deformations at various points within the medium are estimated where no failure of soil is implied.

The methods that are generally adopted for estimating the collapse load of classical stability problems (bearing capacity of footings, earth pressure problems and stability of slopes) in soil mechanics are :

1. Limit equilibrium methods
2. Slip line method
3. Limit analysis

Singh et-al (1995) have presented an annotated bibliography of these methods. Therefore these are not presented here for the sake of brevity.

Limit equilibrium methods have been used to find approximate solutions to stability problems in soil mechanics. Even though the method is not correct from the viewpoint of the theory of plasticity with its incorrectly oriented slip surfaces, it has acquited itself quite well over the years. This simplified approach makes it possible

to solve various problems by using simple statics wherein assumptions regarding the stress distribution along the slip surface are made to arrive at an overall equation of equilibrium in terms of stress resultants. The method basically gives no consideration to kinematics, and equilibrium conditions are satisfied only in a limited sense.

In the slip-line method (Sokolovskii, 1965) at the instant of impending plastic flow, both equilibrium and yield conditions are satisfied in the region near foundation. Coulomb criterion is combined with equilibrium equations to develop a set of differential equations of plastic equilibrium in this region. With suitable transformations it is convenient to integrate these equations along characteristic lines which coincide with the directions of failure or slip lines. For plane problems the two available differential equations and the yield condition produce the sufficiency condition for static determinacy in the sense that there are same number of equations as unknown stress components. The stress field so obtained has been termed as partial stress field as it can't be extended beyond the plastic zone.

With the assumption of ideal plasticity and use of limit theorems (Drucker et-al, 1952) it is possible to find the upper and lower bounds of the collapse load. In contrast to limit equilibrium methods and slip- line method, limit analysis method considers the stress-strain relation in an idealized manner (flow rule considering normality condition). Many solutions to stability problems from the upper bound approach are available in literature. But very few lower bound solutions are available for such problems. It is due to the fact that it is easier to construct a kinematically admissible velocity field in comparison to the statically admissible stress field. Chen (1975) presented a general method of estimating the lower bound solutions of bearing capacity problems. However, the method is complicated and is not generally used.

Lysmer (1970) proposed a very general method of finding the lower bound solution of plane problems using finite elements and optimization (linear programming) method. Since than several variations (Bottero et-al, 1980; Sloan. 1988) and modification (Basudhar, 1976, Basudhar et-al, 1979) have been reported. Bottero et-al generated the statically admissible stress field in a different way but used linear programming in isolating the stress field. As such, they had to adopt the same scheme of successive linearization of the yield criterion. Sloan (1988) further improved upon

the numerical efficiency of the method using a different technique. Basudhar (1976) used the Lysmer (1970) formulation in developing the stress field satisfying the element equilibrium and the interface equilibrium but used non-linear programming technique to isolate the optimal stress field. In this approach therefore, there is no necessity of linearizing the non-linear yield condition. Munro (1982) also suggested a method to find the lower bound solution of plane problems based on finite elements and linear programming. The method was further developed by Chuang (1992 a, b). For rigid elements this method has been claimed to yield upper bound solution.

Chen (1975) recognized the merit of the Lysmer's (1970) scheme in solving such problems. However in this method, for achieving a good solution, recognition of the singular points in generating the mesh of the finite elements is essential. Lysmer (1970) highlighted this aspect in his paper. In modifying Lysmer's method, Basudhar's (1976) main effort was to improve upon the method than to study the effect of the mesh pattern on the solution and its rectification with the help of a general mesh pattern where in the recognition of the singular points was not essential . As such, he took up identical problems and identical mesh patterns as was considered by Lysmer (1970). The studies have been reported by Basudhar et-al (1979, 1980). Subsequently Singh (1992) used Lysmer - Basudhar approach to solve various problems like stability of vertical cuts, reinforced earth walls, horizontal, vertical and inclined anchors, trap doors and bearing capacity of footings over voids. For bearing capacity studies both surface and embedded footings were considered. He observed that the solutions were strongly dependent on the mesh patterns.

Even though the method proposed by Bottero et-al (1980) differed from that of Lysmer (1970) in generating static stress field they were similar in finding the optimal solution by using linear programming. The Bottero et-al method was further improved by Sloan (1988). The type of mesh that has been used by Sloan in solving stability of trap doors strongly suggests that there is no necessity of specially considering the singular points in generating the mesh pattern. However, Sloan (1988) recognized the merit of the original Lysmer's approach (1970) over their method as in the first formulation lesser number of stress variables were to be handled.

handled.

As such it is felt that while using modified Lysmer's method (Basudhar et.al,1979) there is a great need to look into the aspect of achieving solution which are not mesh - dependent. With this in view an effort is made in this thesis to generate a general mesh pattern in arriving at the optimal solution using the Lysmer-Basudhar approach.

The scope and organization of the present thesis is presented in brief as follows :

- In chapter 2 the original formulation of modified Lysmer approach adopted in this thesis for analyzing the various stability problems, has been presented.
- In chapter 3 studies pertaining to the bearing capacity of smooth footing resting either on a cohesive or cohesive-frictional soil and development of a generalized mesh pattern, have been presented. The soil has been assumed to be homogeneous. The obtained results have been compared with solutions available in literature.
- In chapter 4, similar studies for a horizontally stratified two layered soil profile has been presented. Where as, in chapter 5 the soil profile under consideration is vertically stratified.
- In chapter 6 scope of future studies has been presented.

Chapter 2

GENERAL METHOD OF ANALYSIS

2.1 General

The generalized method of lower bound limit analysis as developed by Lysmer (1970) and subsequently modified by Basudhar (1976) to incorporate the non-linear no-yield condition constraints directly in the analysis has been adopted for analyzing the problems.

The method generates stress fields which are in equilibrium everywhere and do not violate the Mohr-Coulomb failure criterion at any point inside the soil medium. Furthermore since infinitely many stress fields satisfy these conditions for any given problem, the method is formulated as a mathematical programming problem to isolate stress fields which yield high lower bounds. The stress field that is considered in this method has the property that all stresses vary linearly within each element of some mesh which cover the soil mass under study. For the sake of completeness the method is presented herein in brief.

The first step in the analysis of a typical problem, such as the bearing capacity problem shown in Fig 2.1, is the disretization of the soil mass under consideration into a mesh of finite number of triangular elements. If possible, the zone of influence considered for discretization should be based on previous experimental and theoret-

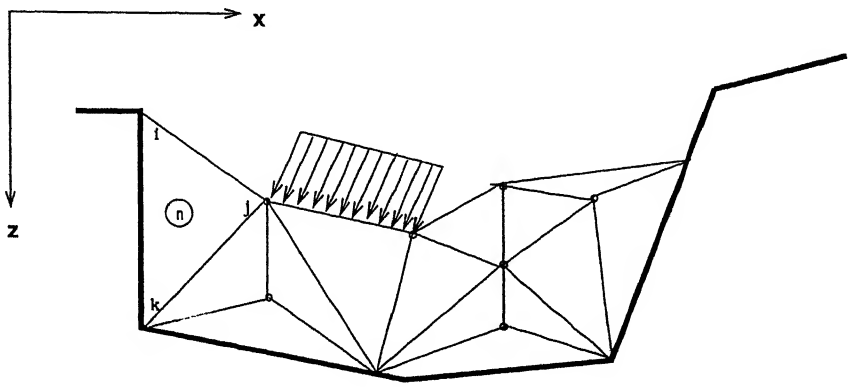

Figure 2.1: Discretization of the soil mass for a typical problem

ical studies. Further discretization of this zone should be done keeping in mind the guide lines suggested by Lysmer (1970). All nodal points, elements and element sides are then numbered in some arbitrary order. It can be shown that a mesh consisting of p elements connecting at q nodal points will have $p + q - 1$ element sides.

2.2 Element Equilibrium:

The geometry of a typical element n, and the external stresses and the body forces acting on this element are shown in Fig 2.2.

The stresses are assumed to vary linearly within each element, hence the stresses,only at the nodes,are considered. In addition, one internal stress σ^n is defined as the normal stress at node i acting on a plane parallel to the side jk. The normal stresses shown in Fig 2.2 are collected into a 7-component stress vector $\{\sigma^n\}$ defined by

$$[\{\sigma\}^n]^T = \{\sigma^n \sigma_{ik} \sigma_{ij} \sigma_{ji} \sigma_{jk} \sigma_{kj} \sigma_{ki}\} \tag{2.1}$$

and the external shear stresses are collected into a 6- component stress vector $\{\tau^n\}$ defined by

$$[\{\tau\}^n]^T = \{\tau_{ik} \tau_{ij} \tau_{ji} \tau_{jk} \tau_{kj} \tau_{ki}\} \tag{2.2}$$

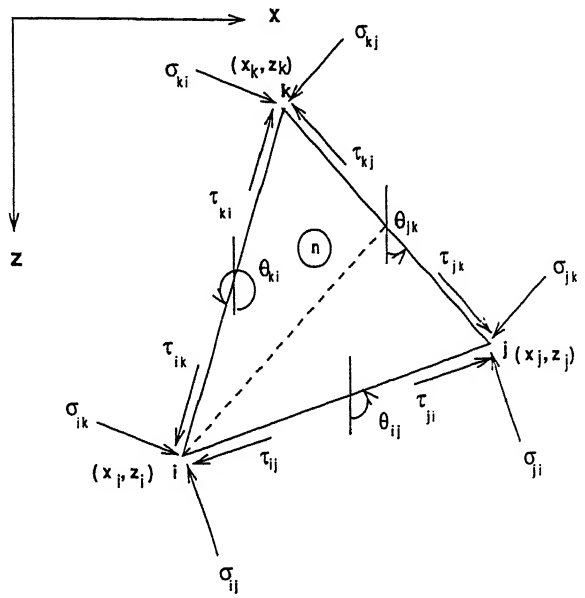

Figure 2.2: Definition sketch and body forces for n th element

the internal stresses in each element are collected into 9-component stress vector $\{s\}$ defined as

$$\{s\}^T = \{\bar{s}_i \bar{s}_j \bar{s}_k\} \tag{2.3}$$

$$\text{with} \{s_i\}^T = \{\sigma_{z,i} \sigma_{x,i} \tau_{zx,i}\} \text{ etc.} \tag{2.4}$$

where $\{\bar{s}_i\}$ are the internal stresses at node i. The equilibrium conditions for the infinitesimal triangle at node i shown in Fig.2.3, are expressed in terms of σ_{ik} and τ_{ik} as:

$$\sigma_{ik} = \sigma_{z,i} \sin^2 \theta_{ik} + \sigma_{x,i} \cos^2 \theta_{ik} - \tau_{zx,i} \sin 2\theta_{ik} \tag{2.5}$$

$$\tau_{ik} = 0.5(\sigma_{x,i} - \sigma_{z,i}) \sin 2\theta_{ik} + \tau_{zx,i} \cos 2\theta_{ik} \tag{2.6}$$

Similar equations are written for nodes j and k and substituted in Eqns. (2.1) and (2.2) to yield

$$\{\sigma\}^n = [s] \tag{2.7}$$

$$\{\tau\}^n = [T] \tag{2.8}$$

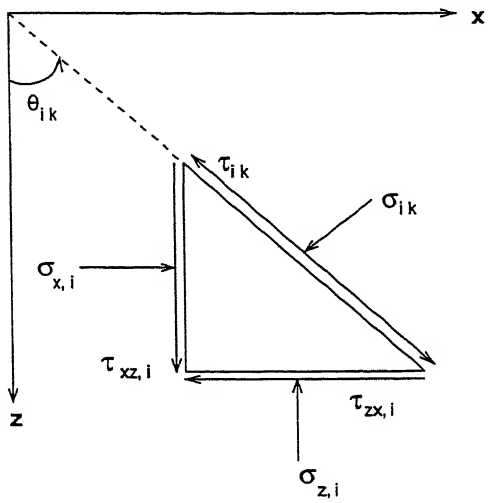

Figure 2.3: Internal stresses at point i

Matrices $[S]$ and $[T]$ are the geometric properties of n th element. The conditions of internal equilibrium are

$$\begin{aligned} \frac{\partial \sigma_z}{\partial z} + \frac{\partial \tau_{zx}}{\partial x} &= \gamma_z \\ \frac{\partial \tau_{zx}}{\partial z} + \frac{\partial \sigma_x}{\partial x} &= \gamma_x \end{aligned} \tag{2.9}$$

To satisfy these relations, the linear stress fields within the n th element are expressed in the following form:

$$\begin{aligned} \sigma_z &= c_1 z + c_2 x + c_3 + \gamma_z z \\ \sigma_x &= c_4 z + c_5 x + c_6 + \gamma_x x \\ \tau_{zx} &= -c_5 z - c_1 x + c_7 \end{aligned} \tag{2.10}$$

Thus the stress field depends on seven parameters c_i which may be combined into the vector

$$\{c\}^T = \{c_1\ c_2\ c_3\ c_4\ c_5\ c_6\ c_7\} \tag{2.11}$$

Using Eqns. (2.3), (2.4) and (2.10) the stress vector $\{s\}$ can be written as:

$$\{s\} = [G]\{c\} + \{g\} \tag{2.12}$$

where

$$\{g\}^T = \{\gamma_z z_i,\ \gamma_x x_i,\ 0,\ \gamma_z z_j,\ \gamma_x x_j,\ 0,\ \gamma_z z_k,\ \gamma_x x_k,\ 0\} \tag{2.13}$$

is purely a function of geometric properties of n th element. Using equns. (2.7) and (2.12),

$$\{c\} = ([S][G])^{-1}\{\sigma\}^n - ([S][G])^{-1}[S]\{g\} \tag{2.14}$$

which when substituted into Eqn. (2.12) gives

$$\{s\} = [B]\{\sigma\}^n + \{h\} \tag{2.15}$$

$$\text{where } [B] = [G]([S][G])^{-1} \text{ and } \{h\} = \{g\} - [B][S]\{g\} \tag{2.16}$$

Both $[B]$ and $\{h\}$ are geometric properties of n th element. Using Eqns. (2.8) and (2.15)

$$\{\tau\}^n = [T][B]\{\sigma\}^n + [T]\{h\} \tag{2.17}$$

which is the equilibrium condition for n th element.

2.3 Interface Equilibrium:

The elements of $\{\sigma\}^n$ vectors for all the elements are collected into a general $\{\sigma\}$ vector. A system consisting of p elements connected at q nodal points will have $(3p + 2q - 2)$ stress variables in $\{\sigma\}$ vector, which are the principal unknowns.

The continuity of normal and shear stresses across any interface as shown in Fig. 2.4 requires:

$$\sigma_{ij}^m = \sigma_{ij}^n \qquad and \qquad \tau_{ij}^m = \tau_{ij}^n \tag{2.18}$$

for all corresponding values of i, j, m and n. These conditions yield a set of linear equality constraints in terms of the principal unknowns. The total number of interface equilibrium conditions is equal to twice the number of element sides in contact.

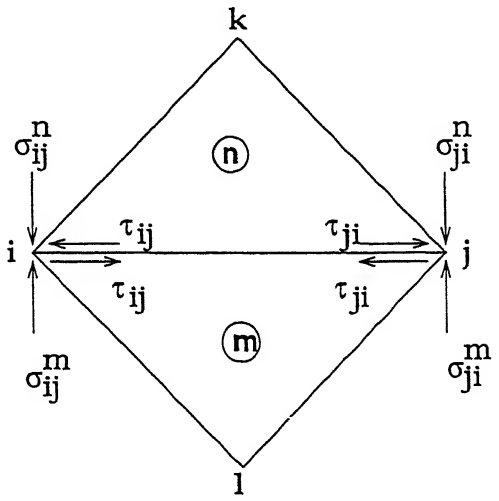

Figure 2.4: Continuity of nodal stresses

2.3 External Boundary Conditions:

The boundary stresses on the external faces of the system may be expressed either as :

$$\tau_{ij} \leq \mu\sigma_{ij}$$

$$\sigma_{ij} = \zeta \qquad and/or \qquad \tau_{ij} = \epsilon\sigma_{ij} \tag{2.19}$$

Eqns. (2.18), and (2.19) can be transformed into the form :

$$\sum_{j=1}^{(3p+2q-2)} a_{ij}\sigma_j = b_i \tag{2.20}$$

and/or

$$\sum_{j=1}^{(3p+2q-2)} a_{ij}\sigma_j \leq b_i \tag{2.21}$$

2.4 No-yield condition:

For static admissibility, the stress field should not violate the Mohr-Coulomb yield criterion at any point in the soil medium. Since all stresses are assumed to vary

linearly within each element, it is sufficient to satisfy the no yield condition at the element corners only. The condition at the node i can be written as:

$$(\sigma_{z,i} - \sigma_{x,i})^2 + (2\tau_{zx,i})^2 \leq [(\sigma_{z,i} + \sigma_{x,i})\mathrm{Sin}\phi + 2C\ \mathrm{Cos}\phi]^2 \tag{2.22}$$

Eqn. (2.22) is expressed in terms of the principal unknowns as follows:

$$\sigma_{z,i} = Z_i\{s\}, \sigma_{x,i} = X_i\{s\} \text{ and } \tau_{zx,i} = T_i\{s\} \tag{2.23}$$

where,

$$\begin{aligned} Z_i = &\ (1,\ 0,\ 0,\ 0,\ 0,\ 0,\ 0,\ 0,\ 0) \\ X_i = &\ (0,\ 1,\ 0,\ 0,\ 0,\ 0,\ 0,\ 0,\ 0) \\ T_i = &\ (0,\ 0,\ 1,\ 0,\ 0,\ 0,\ 0,\ 0,\ 0) \end{aligned} \tag{2.24}$$

similarly for nodes j and k ,

$$\begin{aligned} Z_j = &\ (0,\ 0,\ 0,\ 1,\ 0,\ 0,\ 0,\ 0,\ 0) \\ X_j = &\ (0,\ 0,\ 0,\ 0,\ 1,\ 0,\ 0,\ 0,\ 0) \\ T_j = &\ (0,\ 0,\ 0,\ 0,\ 0,\ 1,\ 0,\ 0,\ 0) \end{aligned} \tag{2.25}$$

and

$$\begin{aligned} Z_k = &\ (0,\ 0,\ 0,\ 0,\ 0,\ 0,\ 1,\ 0,\ 0) \\ X_k = &\ (0,\ 0,\ 0,\ 0,\ 0,\ 0,\ 0,\ 1,\ 0) \\ T_k = &\ (0,\ 0,\ 0,\ 0,\ 0,\ 0,\ 0,\ 0,\ 1) \end{aligned} \tag{2.26}$$

Eqns. (2.21) and (2.22) yield:

$$(A_i\{s\})^2 + (2T_i\{s\})^2 - (B_i\{s\}\ \mathrm{Sin}\phi + 2C\ \mathrm{Cos}\phi)^2 \leq 0 \tag{2.27}$$

where

$$\begin{aligned} A_i = &\ (Z_i - X_i) \\ B_i = &\ (Z_i + X_i) \end{aligned} \tag{2.28}$$

Now, Eqn. (2.27) can be rewritten in terms of $\{\sigma\}^n$ as:

$$[A_i([B]\sigma^n + h)]^2 + [2T_i([B]\sigma^n + h)]^2$$
$$-[B_i([B]\sigma^n + h)\sin\phi + 2C\cos\phi]^2 \leq 0 \tag{2.29}$$

Similar relations can be obtained for the nodes j and k. The elements of $\{\sigma\}^n$ vector can be picked up from the general stress vector $\{\sigma\}$. The total number of non-linear equality constraints will be 3p. It is sufficient to satisfy the non–linear equality constraints only at the nodal points of the triangular elements to ensure that there is no yield at any point within the element. The proof of the same had been provided by Lysmer (1993).

2.5 Objective function, Design Variables, Design Restrictions and Reduction of Design Variables:

Since in general infinitely many stress fields will satisfy the aforementioned conditions of static admissibility, the isolation of the stress field which optimizes the objective function is important. In almost all the problems, the stress quantity is a linear combination of surface stresses σ_{ij} and τ_{ij}. Using Eqn. (2.17) this quantity can be transformed into a linear combination of principal unknown σ_j which are termed as design variables. The problem can be stated as:

$$\text{OPTIMIZE} \sum_j a_j\sigma_j \tag{2.30}$$

The design restrictions are interface equilibrium and the external boundary conditions. As soil cannot take tension, the following constraints are also introduced,

$$-\sigma_j \leq 0 \tag{2.31}$$

Eqns. (2.20) and (2.28) are presented in general form as:

$$g_j \leq 0 \tag{2.32}$$

The equality constraints (Eqn. 2.20) can be rewritten in matrix notation as

$$[\mathrm{A}]\{\sigma\} = \{b\} \tag{2.33}$$

Some of the elements of $\{\sigma\}$ vector are specified at the boundary. The following relation :

$$[\mathrm{A}^*]\{\sigma^*\} = \{b^*\} \tag{2.34}$$

can be arrived at by eliminating the columns of [A] matrix corresponding to the known elements of the $\{\sigma\}$ vector. $\{\sigma^*\}$ is a vector which is achieved by eliminating the known elements of $\{\sigma\}$ vector. $\{b^*\}$ vector is calculated as follows:

$$\{b^*\} = \{b\} - [\mathrm{A}']\{\sigma'\} \tag{2.35}$$

[A'] matrix contains the columns that are removed from [A] matrix and $\{\sigma'\}$ contains those elements of $\{\sigma\}$ vector that are specified.

The following steps are performed for the general rectangular matrix [A*]:
Step 1. The rank and the linearly dependent rows and columns if there be any of the given matrix, are determined.
Step 2. A sub matrix of maximal rank is expressed as product of triangular factors.
Step 3. The non basic rows are expressed in terms of the basic ones.
Step 4. The basic variables are expressed in terms of the free variables.

By considering these free variables as design variables and expressing the remaining basic variables in terms of these design variables the equality constraints (Eqn. 2.33) are implicitly satisfied. Such a technique helps in reducing the complexity of the problem by eliminating the equality constraints and there by reducing the dimensionality of the problem. The independent design variables so obtained are collected in **D** vector.

The rank(r) is determined using the standard Gaussian elimination technique with complete pivoting. This implies that the rows and columns of the given $m' \mathrm{x} n'$ matrix [A*] are interchanged at each elimination step if necessary. In general the following cases may arise:

1. $r = m' = n'$

[A*] is non-singular and $[\mathbf{A}^*]\{\sigma^*\} = \{b^*\}$ has uniquely determined solution.

2. $r < m'$

[A*] is not row regular and the solution of Eqn.(2.33) exists only if the remaining $(m' - r)$ equations are linearly dependent.

3. $r < n'$

[A*] is not column regular and the system has no solution.

Cases (1) and (2) may occur combined. The solution if it exits, can be uniquely determined if $r = n'$, otherwise, it contains $(n' - r)$ free parameters.

The basic variables (σ^{**}) are expressed in terms of the free design variable (**D**) as follows :

Once the steps 1,2 and 3 of the enunciated reduction process are carried out Eqn. (2.34) is reduced to a form,

$$[\mathbf{A}^*]^r\{\sigma^*\}^r = \{b^*\}^r \tag{2.36}$$

where the superscript denotes the r th elimination step and

$$[\mathbf{A}^*]^r = \begin{pmatrix} \mathbf{L} \\ \mathbf{LR} \end{pmatrix} (\mathbf{U}, \mathbf{UR}) \tag{2.37}$$

where L is a unit lower triangular matrix of dimension rxr.

U is a unit upper triangular matrix of dimension rxr.

LR is of dimension $(m' - r)$ r; if the matrix $[A^*]$ is row regular that is $(m' = r)$, **LR** is absent in the final factorization.

UR is of dimension r $(n' - r)$; if the matrix [**A***] is column regular that is $(n' = r)$, **UR** is absent in the final factorization.

Let $\{\sigma^*\}^r$ and $\{b^*\}^r$ be partitioned into

$$\begin{Bmatrix} \sigma^{**} \\ \mathbf{D} \end{Bmatrix} \quad and \quad \begin{Bmatrix} b_1^* \\ b_2^* \end{Bmatrix}$$

Then for a consistent system of equations

$$\sigma^{**} = \mathbf{U}^{-1}\mathbf{L}^{-1}b^* + \mathbf{HD} \tag{2.38}$$

$$\text{where} \qquad \mathbf{H} = -\mathbf{U}^{-1}\mathbf{U}\mathbf{R} \tag{2.39}$$

$$\text{and} \qquad b_1^* = \mathbf{L}\mathbf{U}\sigma^{**} + \mathbf{L}\mathbf{U}\mathbf{R}\mathbf{D} \tag{2.40}$$

$$b_2^* = \mathbf{L}\mathbf{R}\mathbf{L}^{-1}b_1^* \tag{2.41}$$

In the present thesis subroutine MFGR developed by IBM has been used to perform the calculations enunciated in steps 1 to 4 of the reduction process.

2.6 Mathematical Programming Problem:

Determination of the minimum value of the objective function subject to the inequality constraints as described above is formulated as a mathematical programming problem which is stated as follows:

Find $\mathbf{D_m}$ such that

$$F(\mathbf{D_m}) = \Sigma \mathbf{a_j}\sigma_\mathbf{j} \qquad \text{is minimum} \tag{2.42}$$

subject to $g_j(\mathbf{D_m}) \leq \mathbf{0}$

There is no loss of generality even though the problem is cast as a minimization problem as maximum of a function can be achieved by minimizing the negative of the function.

The constrained problem is converted into an unconstrained optimization problem with the help of extended penalty function technique as suggested by Kavlie and Moe (1971). The Sequential Unconstrained Minimization of the developed composite function is carried out using Powell's conjugate direction algorithm (Powell, 1964) along with Quadratic interpolation technique for linear minimization to isolate the optimal solution. These methods are available in any standard text book on Optimization (Fox, 1971; Rao, 1984). The composite function $\phi(\mathbf{D}, r_k)$ is developed by blending the objective function and constraints as follows:

$$\phi(\mathbf{D}, r_k) = F(\mathbf{D}) + r_k \sum_{j=1}^{M} \mathbf{G}[g_j(\mathbf{D})] \tag{2.43}$$

The function $G[g_j(\mathbf{D})]$ is chosen as:

$$G[g_j(\mathbf{D})] = \left\{ \begin{array}{ll} 1/g_j(\mathbf{D}) & g_j(\mathbf{D}) \leq 0 \\ 2\lambda - g_j(\mathbf{D})/\lambda^2 & g_j(\mathbf{D}) \geq \lambda \end{array} \right\} \tag{2.44}$$

where $\lambda = -r_k/\delta_t$

and $\delta_t = a$ constant that defines the transition between the two types of penalty terms.

In this approach infeasible starting points are readily acceptable to the minimization algorithm, which makes it a powerful technique for solving various engineering problems even if an initial feasible design vector is difficult to guess.

Chapter 3

Footing On Homogeneous Cohesive and Cohesive-frictional Soil

3.1 Introduction

Srivastava (1993) used extended Lysmer's approach (Basudhar et.al , 1979) and compared the solutions obtained with the Sloan's solution (1988) and Chuang's solution (1992). He has found that the the solutions are in close agreement. However, the mesh adopted by him, was not a general one. Starting with the mesh pattern adopted by him in this chapter an effort has been made to generalize the mesh pattern for homogeneous soils to determine the bearing capacity of strip footings resting on either cohesive or cohesive-frictional soils.

3.2 The Problem

Fig.3.1 shows a smooth strip footing resting on the surface of a cohesive frictional ($C - \phi$) soil.The objective is to determine the bearing capacity factors N_q and N_c values for cohesive-frictional soils as well as N_c values for cohesive soils only.

The exact collapse pressure for a smooth strip footing resting on the surface of a cohesive-frictional weightless soil may be written as :

$$q_f = CN_c + q.N_q \tag{3.1}$$

As per Prandtl's solution

$$N_q = \exp(\pi \tan \phi) \tan^2(\pi/4 + \phi/2) \tag{3.2}$$

$$N_c = (N_q - 1) \cot \phi \tag{3.3}$$

From the above relations N_q can be obtained as follows:

$$N_q = \frac{q_f}{C \cot \phi} + 1 \tag{3.4}$$

where q is overburden pressure.Prandtl has assumed the soil mass to be homogeneous, isotropic and weightless.

3.3 The Objective Function

The objective function is $-(\sigma_{12} + \sigma_{21})$. Bearing capacity is equal to half of the absolute value of the objective function.

3.4 The Boundary Conditions

The boundary conditions for the meshes shown for the various figures are as follows :

For Net-1 and Net-1.extended

$\sigma_{1,20} = \sigma_{20,1} = 0.0$ (*boundary condition*)

$\tau_{1,20} = \tau_{20,1} = 0.0$ (*boundary condition*)

$\tau_{1,2} = \tau_{2,1} = 0.0$ (*smooth footing*)

and $\tau_{2,3} = \tau_{3,2} = \tau_{3,4} = \tau_{4,3} = \tau_{4,5} = \tau_{5,4} = \tau_{5,6} = \tau_{6,5} = 0.0$ (*symmetry condition*)

In addition to the above two more symmetry conditons are required for Net-1.extended,

$$\tau_{6,7} = \tau_{7,6} = 0.0$$

For Net-2, Net-2.1, Net-3, Net-3.ext.1, Net-3.ext.2 and Net-3.ext.3 the following conditions are common :

$$\sigma_{2,3} = \sigma_{3,2} = 0.0 \qquad (boundary \quad condition)$$

$$\tau_{2,3} = \tau_{3,2} = 0.0 \qquad (boundary \quad condition)$$

$$\tau_{1,2} = \tau_{2,1} = 0.0 \qquad (smooth \quad footing)$$

3.5 Results and Discussions

As already stated Srivastava (1993) had demonstrated the effectiveness of the Lysmer-Basudhar (Basudhar et.al, 1979) technique by solving a particular test case with $C = 1.00$ kPa and $\phi = 40^0$. The mesh taken by Srivastava (1993), is as indicated in Fig 3.1.(a) (referred as Net.1).

But the solution of Srivastava (1993) lacked on two counts:

1. In general the magnitude of principal stress variables developed in the elements, as one move from the element 1 supporting the strip footing on the element side (1,2) towards the element with the free boundary side (2,3) should be decreasing. However, in the stress field reported by Srivastava (1993), some of the stress variables did not follow this trend. In Table 3.1 the underlined stress variables are in question. This may be either due to the fact that the nodal point 2 is a singularity point or due to the premature termination of the computations.

2. It can be seen from Fig. 3.1.(a), Net-1, that the mesh pattern is influenced by the possible failure geometry even though it does not follow any particular shape like a circle or logarithmic spiral.

The following studies have been conducted for greater understanding of these aspects. The original mesh of Srivastava (1993) could not be studied as the mesh co-ordinate points had not been tabulated and as such, to reproduce the same as best as possible, the co-ordinate values of the mesh node points were measured from the figures presented in his thesis.

The obtained results are presented in Table 3.2. The results show that the type of discrepancy observed by Srivastava are absent. However, for the 18 elements mesh pattern, the obtained value of the bearing capacity factor N_q (61.68) is marginally less than that (62.42) reported by Srivastava (1993), the difference being only 1.185%.

It is therefore concluded that the reasons for anomally in the results as reported by Srivastava could be due to premature termination of the computations. The singular nature of the nodal point 2 did not play any significant role in this.

Next, an effort is made to develop a generalized mesh pattern for finding the critical load which does not require any special knowledge of the probable failure surface.

The studies were made as follows :-

1. The mesh pattern as suggested by Srivastava (1993) was extended over a rectangular domain as shown in Fig 3.1.(b),Net-1.ext. But with this no feasible solution could be obtained.

2. Srivastava (1993) chose his mesh pattern roughly based on the Hill's surface considering only the half width of the footing. As this procedure did not work an asymmetric mesh pattern with 15 elements was chosen (following Prandtl's surface) as shown in Fig 3.2.(a), Net-2. Studies have been conducted with cohesive as well as general cohesive-frictional soils. Solutions were obtained for $C = 1$ kPa and ($\phi = 0^0$). The obtained N_c value is 5.0278 in comparison to the upper bound solution of 5.18(Chuang 1993) and 5.1416 (Prandtl's exact solution) .

Table 3.1

Stress Field and Stress-Strength Ratios at the Nodal Points for Net-1

15 element net as presented by Srivastava (1993)

Element No.	Nodal Point	σ_x	σ_z	τ_{zx}	Stress Strength ratio
1	1	15.4204	71.2003	0.0000	0.9506
1	2	15.4204	75.2055	0.0000	0.9999
1	3	15.4205	75.2055	0.0000	0.9999
2	1	15.3154	71.1834	0.0420	0.9562
2	3	15.4205	75.2055	0.0000	0.9999
2	4	15.5256	75.1887	0.0000	0.9940
3	1	14.4538	70.6321	0.7312	0.9990
3	4	15.5256	75.1887	0.0000	0.9940
3	5	16.1955	74.8230	0.0000	0.9535
4	1	15.9511	73.1624	1.2151	0.9479
4	5	16.1955	74.8231	0.0000	0.9535
4	6	16.2371	75.6737	0.0000	0.9568
5	1	12.9328	61.0891	4.8215	0.9999
5	6	14.0811	66.6897	4.4919	0.9962
5	7	13.3008	60.0142	6.6437	0.9962
6	1	11.6547	40.6404	9.9336	0.9996
6	7	12.4963	47.1428	9.8615	0.9999
6	8	12.3571	38.0969	11.0273	0.9960
7	1	11.5977	29.4715	10.7314	0.9999
7	8	12.3380	34.3410	11.2956	0.9999
7	9	12.3189	26.8534	11.1751	0.9961
8	1	11.5690	23.0060	10.3004	0.9837
8	9	12.3107	25.0217	11.0529	0.9977
8	10	12.2371	23.1742	10.7112	0.9802
9	1	11.1911	12.2577	8.2851	0.9991
9	10	11.9035	13.6866	8.9322	0.9969
9	11	11.6153	11.4019	8.1628	0.9999

contd. on next page

Table 3.1

Element No.	Nodal Point	σ_x	σ_z	τ_{zx}	Stress Strength ratio
10	1	10.1463	6.5225	5.8372	0.9962
10	11	11.0244	8.1584	6.7784	0.9991
10	12	10.2865	5.7454	5.4532	0.9944
11	1	9.2873	4.2026	4.4225	0.9999
11	12	9.9722	4.9095	4.9378	0.9999
11	13	9.3521	3.7494	4.1065	0.9976
12	1	8.2344	2.5191	3.0935	0.9949
12	13	8.8583	2.9570	3.4809	0.9999
12	14	8.2551	2.2618	2.8439	0.9928
13	1	6.8313	1.1160	1.6904	0.9999
13	14	7.4100	1.4167	1.9988	0.9995
13	15	6.7402	0.9606	1.4557	0.9967
14	1	5.6190	0.4341	0.7811	0.9971
14	15	6.0652	0.5809	0.9494	0.9998
14	16	5.5468	0.3693	0.6270	0.9971
15	1	4.5396	0.0606	0.1462	0.9997
15	16	4.9581	0.1656	0.2807	0.9998
15	17	4.4038	0.0251	0.0086	0.9999
16	1	4.2531	0.0014	0.0160	0.9929
16	17	4.3484	0.0136	0.0165	0.9995
16	18	4.3044	0.0059	0.0243	0.9981
17	1	4.2787	0.0037	0.0237	0.9955
17	18	4.3218	0.0075	0.0190	0.9997
17	19	4.2870	0.0000	0.0252	0.9998
18	1	4.1285	0.0000	0.0000	0.9728
18	19	4.2873	0.0000	0.0252	0.9998
18	20	4.2884	0.0000	0.0000	0.9999

Table 3.2

Stress Field and Stress-Strength Ratios at the Nodal Points for Net-1

15 element net as per present study (1996)

Element No	Nodal Point	σ_x	σ_z	τ_{zx}	Stress Strength ratio
1	1	0.151167E+02	0.732069E+02	0.762939E-05	0.992629E+00
1	2	0.151167E+02	0.738087E+02	0.381470E-05	0.999990E+00
1	3	0.151170E+02	0.738087E+02	0.000000E+00	0.999974E+00
2	1	0.150295E+02	0.731851E+02	0.436200E-01	0.997265E+00
2	3	0.151170E+02	0.738087E+02	0.762939E-05	0.999973E+00
2	4	0.152046E+02	0.737869E+02	0.381470E-05	0.994817E+00
3	1	0.149863E+02	0.731418E+02	0.868752E-01	0.999178E+00
3	4	0.152046E+02	0.737869E+02	0.762939E-05	0.994816E+00
3	5	0.153793E+02	0.737174E+02	0.381470E-05	0.984275E+00
4	1	0.149409E+02	0.729948E+02	0.168556E+00	0.999961E+00
4	5	0.153793E+02	0.737174E+02	0.762939E-05	0.984272E+00
4	6	0.155742E+02	0.735825E+02	0.762939E-05	0.971902E+00
5	1	0.125028E+02	0.565136E+02	0.650747E+01	0.999994E+00
5	6	0.126949E+02	0.541187E+02	0.748607E+01	0.980648E+00
5	7	0.127672E+02	0.565604E+02	0.696857E+01	0.994043E+00
6	1	0.117257E+02	0.408663E+02	0.999458E+01	0.999997E+00
6	7	0.120759E+02	0.426417E+02	0.100705E+02	0.994618E+00
6	8	0.120205E+02	0.401140E+02	0.103818E+02	0.993744E+00
7	1	0.116681E+02	0.299511E+02	0.107878E+02	0.999711E+00
7	8	0.119769E+02	0.318477E+02	0.109825E+02	0.994444E+00
7	9	0.119779E+02	0.287238E+02	0.109892E+02	0.995422E+00
8	1	0.116543E+02	0.239791E+02	0.105011E+02	0.993031E+00
8	9	0.119692E+02	0.249712E+02	0.108091E+02	0.996050E+00
8	10	0.119364E+02	0.232486E+02	0.106105E+02	0.991678E+00
9	1	0.113437E+02	0.135750E+02	0.870355E+01	0.999999E+00
9	10	0.116863E+02	0.148698E+02	0.916288E+01	0.999809E+00
9	11	0.114659E+02	0.125953E+02	0.846860E+01	0.997236E+00

contd. on next page

Table 3.2

Element No.	Nodal Point	σ_x	σ_z	τ_{zx}	Stress Strength ratio
10	1	0.102289E+02	0.673456E+01	0.594204E+01	0.992163E+00
10	11	0.106483E+02	0.757853E+01	0.644333E+01	0.999875E+00
10	12	0.103262E+02	0.650727E+01	0.586300E+01	0.996728E+00
11	1	0.954860E+01	0.470452E+01	0.476688E+01	0.999998E+00
11	12	0.998155E+01	0.547882E+01	0.526765E+01	0.997796E+00
11	13	0.946084E+01	0.441732E+01	0.452553E+01	0.982591E+00
12	1	0.842041E+01	0.270940E+01	0.326658E+01	0.997984E+00
12	13	0.848969E+01	0.269990E+01	0.323406E+01	0.990007E+00
12	14	0.839712E+01	0.253365E+01	0.311311E+01	0.998668E+00
13	1	0.711665E+01	0.131994E+01	0.192065E+01	0.999694E+00
13	14	0.747400E+01	0.154984E+01	0.216013E+01	0.999903E+00
13	15	0.692258E+01	0.112578E+01	0.168083E+01	0.998671E+00
14	1	0.563924E+01	0.452720E+00	0.788734E+00	0.990179E+00
14	15	0.593933E+01	0.548633E+00	0.927512E+00	0.999463E+00
14	16	0.559302E+01	0.406610E+00	0.710361E+00	0.995886E+00
15	1	0.452261E+01	0.549333E-01	0.122266E+00	0.999949E+00
15	16	0.482584E+01	0.133315E+00	0.252473E+00	0.999934E+00
15	17	0.439927E+01	0.251405E-01	0.397624E-01	0.999454E+00
16	1	0.430989E+01	0.103730E-01	0.249060E-01	0.995691E+00
16	17	0.432705E+01	0.100103E-01	0.670129E-02	0.998687E+00
16	18	0.426082E+01	-0.547647E-02	0.220390E-01	0.999603E+00
17	1	0.418024E+01	-0.286419E-02	0.165205E-01	0.983931E+00
17	18	0.426140E+01	-0.541694E-02	0.218491E-01	0.999653E+00
17	19	0.428840E+01	0.293106E-04	0.215831E-02	0.999876E+00
18	1	0.427551E+01	0.000000E+00	0.166869E-05	0.997747E+00
18	19	0.428740E+01	-0.461936E-06	0.233147E-02	0.999732E+00
18	20	0.428896E+01	0.000000E+00	0.953674E-06	0.999992E+00

3. The Net-2 was then extended in sequence as shown in Fig 3.2.(a) and Fig 3.2.(b) to arrive at a general mesh pattern over a rectangular domain,as shown in Fig 3.3 (a), (Net-3). All these meshes produced very good results (5.0278, 5.0266, 5.0286 and 5.048) for N_c, that were very close to Prandtl's solution (5.1416) differing only by 1.82%, (Net-3) to 2.24% (Net-2.Ext.1). It can be seen that the best solution (5.048) has been obtained by the general mesh (Net-3). The complete stress field obtained for the Net-3 is presented in Table-3.3. It can be seen from the table that the obtained stress- strength ratio at different nodal points for most of the elements are almost close to unity thus signifying that the solution is close to the limiting equilibrium state.

4. Studies regarding the extensibility of Net-3 was conducted. As indicated by dotted lines in Fig-3.3(a), two extended nets, Net-3.ext.1 and Net.3.ext.2 were taken up to study the extensibility in the vertical direction as well as the horizontal direction. The N_c value of 5.026 and 5.0257 found for those nets were only 0.44% and 0.442% lower than the value obtained by the original generalized net. But here as an asymmetric net was considered the horizontal extensibility of the net in one direction alone was not sufficient. So the extensibility of the net in the other direction also had to be ascertained.

5. For studying further horizontal extensibility of Net-3, Net.3.ext.3, (Fig-3.3(b)), was taken up, where in the elements 1 to 4 were extended. An extra element as indicated by dotted line was also added, but with that no solution could be achieved. So the extra element of the net was discarded and further studies were conducted by extending the mesh as shown in Fig-3.3(b) and also by varying the z-coordinates (d, as indicated in Fig-3.3(b)) of the nodal point 17. An N_c value of 5.01 differing by only 0.753% was obtained and corresponding to the d values of 0.125m, 0.05m and 0.01m, the N_c values were 4.98, 4.897 and 4.85 respectively. These values are lower than the previously obtained value of 5.048 corresponding to the suggested generalized mesh pattern, the maximum difference being only 2.91% . So for all practical purposes the stress field may be considered to be extensible.

Table 3.3

Stress Field and Stress-Strength Ratios at the Nodal Points for Net-3

15 element net.

Element No.	Nodal Point	σ_x	σ_z	τ_{zx}	Stress Strength ratio
1	2	0.307130E+01	0.505004E+01	0.162172E-02	0.978864E+00
1	1	0.304834E+01	0.504709E+01	0.151253E-02	0.998754E+00
1	17	0.304748E+01	0.504705E+01	0.709629E-02	0.999623E+00
2	2	0.330771E+01	0.508329E+01	0.870342E-01	0.795741E+00
2	17	0.305070E+01	0.504750E+01	0.830555E-02	0.996874E+00
2	16	0.309981E+01	0.508943E+01	0.781240E-01	0.995752E+00
3	2	0.301443E+01	0.498632E+01	0.816016E-01	0.978750E+00
3	16	0.309860E+01	0.508902E+01	0.774269E-01	0.996445E+00
3	15	0.298154E+01	0.496217E+01	0.256519E-01	0.981378E+00
4	2	0.293742E+01	0.490932E+01	0.158609E+00	0.997254E+00
4	15	0.295615E+01	0.493678E+01	0.510416E-01	0.983332E+00
4	14	0.270325E+01	0.458916E+01	0.317988E+00	0.990283E+00
5	2	0.257763E+01	0.380746E+01	0.788240E+00	0.999442E+00
5	14	0.250798E+01	0.399115E+01	0.659706E+00	0.985163E+00
5	13	0.246041E+01	0.359009E+01	0.823282E+00	0.996836E+00
6	2	0.253804E+01	0.294519E+01	0.973013E+00	0.988196E+00
6	13	0.243475E+01	0.303113E+01	0.943058E+00	0.978277E+00
6	12	0.243469E+01	0.280416E+01	0.973279E+00	0.981399E+00
7	2	0.253804E+01	0.258361E+01	0.973013E+00	0.947273E+00
7	12	0.243469E+01	0.250011E+01	0.973279E+00	0.948342E+00
7	11	0.243465E+01	0.222388E+01	0.984612E+00	0.980567E+00
8	2	0.251504E+01	0.133520E+01	0.803584E+00	0.993756E+00
8	11	0.242422E+01	0.165722E+01	0.907706E+00	0.971000E+00
8	10	0.239248E+01	0.125250E+01	0.799875E+00	0.964685E+00
9	2	0.251309E+01	0.131345E+01	0.797059E+00	0.995085E+00
9	10	0.239178E+01	0.124470E+01	0.797535E+00	0.965010E+00
9	9	0.238220E+01	0.110310E+01	0.765862E+00	0.995565E+00

contd. on next page

Table 3.3

Element No.	Nodal Nodal	σ_x	σ_z	τ_{zx}	Stress Strength ratio
10	2	0.237483E+01	0.651847E+00	0.494612E+00	0.986805E+00
10	9	0.229744E+01	0.697519E+00	0.580451E+00	0.976858E+00
10	8	0.225669E+01	0.604642E+00	0.528859E+00	0.962003E+00
11	2	0.221218E+01	0.275205E+00	0.247105E+00	0.999027E+00
11	8	0.212830E+01	0.307336E+00	0.333485E+00	0.940188E+00
11	7	0.208218E+01	0.264555E+00	0.297110E+00	0.914216E+00
12	2	0.198974E+01	0.910398E-02	0.381214E-02	0.980743E+00
12	7	0.207857E+01	0.260226E+00	0.293154E+00	0.912529E+00
12	6	0.201087E+01	0.321137E+00	0.291445E+00	0.798740E+00
13	2	0.196425E+01	-0.104121E-01	0.184919E-01	0.975163E+00
13	6	0.149092E+01	-0.769489E-01	0.163512E+00	0.641287E+00
13	5	0.165806E+01	-0.290776E-01	0.827224E-01	0.718450E+00
14	2	0.197510E+01	-0.526583E-02	0.110201E-01	0.980579E+00
14	5	0.185482E+01	0.642993E-01	0.528232E-01	0.804282E+00
14	4	0.150681E+01	-0.104867E+00	0.212306E+00	0.694453E+00
15	2	0.199816E+01	0.000000E+00	0.193715E-06	0.998161E+00
15	4	0.196621E+01	0.596046E-07	0.718507E-02	0.966551E+00
15	3	0.198312E+01	0.000000E+00	0.596046E-07	0.983193E+00

6. For the study of the convergence, the same mesh pattern suggested by Net-3 was also tried with a lesser number of elements. It was found to give satisfactory results with 14, 13 and 12 element meshes also. The N_c values obtained for the 14, 13 and 12 element meshes were 4.94, 4.923, and 4.927 respectively which were lower than Prandtl's solution by only 3.92%, 4.25% and 4.17% respectively. However, for 11 and 10 element meshes the N_c values obtained were too low. It can be concluded that the generalized mesh pattern with number of elements less than 12 gives non optimal lower bound solution. It can be said that the maximum lower bound solution (bearing capacity factor N_c) of strip footing supported over a homogeneous clay converged to a value of 5.05.

All the N_c values obtained by the various meshes has been tabulated and shown in Table-3.4.

Table 3.4

N_c VALUES OBTAINED BY DIFFERENT MESH PATTERNS

Net name	Number of elements	Figure No.	Lower Bound N_c value	diff. from Prandtl's N_c value
Net-1	18	Fig.3.1(a)	5.016	2.44%
Net-2	15	Fig.3.2(a)	5.028	2.21%
Net-2.ext.1	15	Fig.3.2(a)	5.0266	2.24%
Net-2.ext.2	15	Fig.3.2(b)	5.0286	2.19%
Net-3	15	Fig.3.3(a)	5.048	1.82%
Net-3.ext.1	15	Fig.3.3(a)	5.0266	2.24%
Net-3.ext.2	15	Fig.3.3(a)	5.0257	2.25%
Net-3.ext.3	15	Fig.3.3(b)	5.0100	2.56%
Net-3.ext.3(i)	15	Fig.3.3(b)	4.980	3.14%
Net-3.ext.3(ii)	15	Fig.3.3(b)	4.897	4.76%
Net-3.ext.3(iii)	15	Fig.3.3(b)	4.850	5.67%
Net-4	14	--	4.942	3.88%
Net-5	13	--	4.923	4.25%
Net-6	12	--	4.927	4.17%

It can be observed from Table-3.4 that for all the meshes studied the maximum and minimum percentage difference from the Prandtl's exact solution (5.1416) are 5.67% (Net-3.ext.3(iii)) and 1.82% (Net-3,Fig 3.3(a)) respectively. However, the percentage difference between the minimum and maximum lower bound solution is only 3.9%. This is for all purposes negligible fromthe practical point of view though theoretically the difference is significant.

Srivastava (1993) made a very limited study for predicting the N_q values for a general ($C - \phi$) soil. To study the effect of variation of ϕ on the N_q values for the chosen mesh patterns (Net 1 to Net 3), ϕ has been varied from 10^0 to 40^0. The results are presented in Table 3.5 as well as in Fig 3.4. The study shows that the obtained results are in close agreement with each other and differ from the Prandtl's solution by 1.11% to 6.63% on the safer side, whereas Chuang's (1992) solution corresponding to ($\phi = 30^0$), differs by 0.625% from the Prandtl's solution on the unsafe side. It should

be noted that both Prandtl's and Chuang's rigid elements solutions are upper bound solutions.

A study was also made considering three elements in the zone connecting the right corner of the footing, right bottom most and the the right top most corners of the rectangular domain (ref Fig-3.5) instead of two elements only in that zone. For this case no solutions could be obtained even after several iterations. This indicates that not more than two elements should be considered in those zones.

Table 3.5 N_q VALUES FOR $(C - \phi)$ SOIL

Net Used	C=1kPa $\phi = 10^0$	Diff from Prandtl	C=1kPa $\phi = 20^0$	Diff from Prandtl	C=1kPa $\phi = 30^0$	Diff from Prandtl	C=1kPa $\phi = 40^0$	Diff from Prandt
Net-1	2.42	2.02%	6.27	2.02%	17.85	2.99%	61.415	4.34%
Net-2	2.39	3.23%	6.18	3.42%	18.13	1.47%	63.275	1.44%
Net-3	2.43	1.49%	6.20	3.11%	17.18	6.63%	63.487	1.11%
Chuang	--	--	--	--	18.515	−0.625%	--	--
Prandtl	2.47		6.399		18.40		64.20	

3.6 Conclusions

The following conclusions, based on the presented results and discussions, can be drawn:

1. A general asymmetric mesh pattern (Net-3), could be identified, for obtaining the lower bound solution for the bearing capacity problem for strip footing on homogeneous clay, using extended Lysmer's approach.

2. A horizontal extent of the mesh of about 3.25 B (breadth of the footing) and a vertical extent of 1.5 B was found to be suitable.

3. The number of elements required to be considered, was found to be 15 elements for best result. However, moderately good results could be obtained by even 12 element meshes also.

4. For ($C - \phi$) soil case, the number of elements, in the zone, connecting the right corner of the footing, right bottom most and the right top most corners of the rectangular domain (refer Fig-3.5) should be restricted to 2.

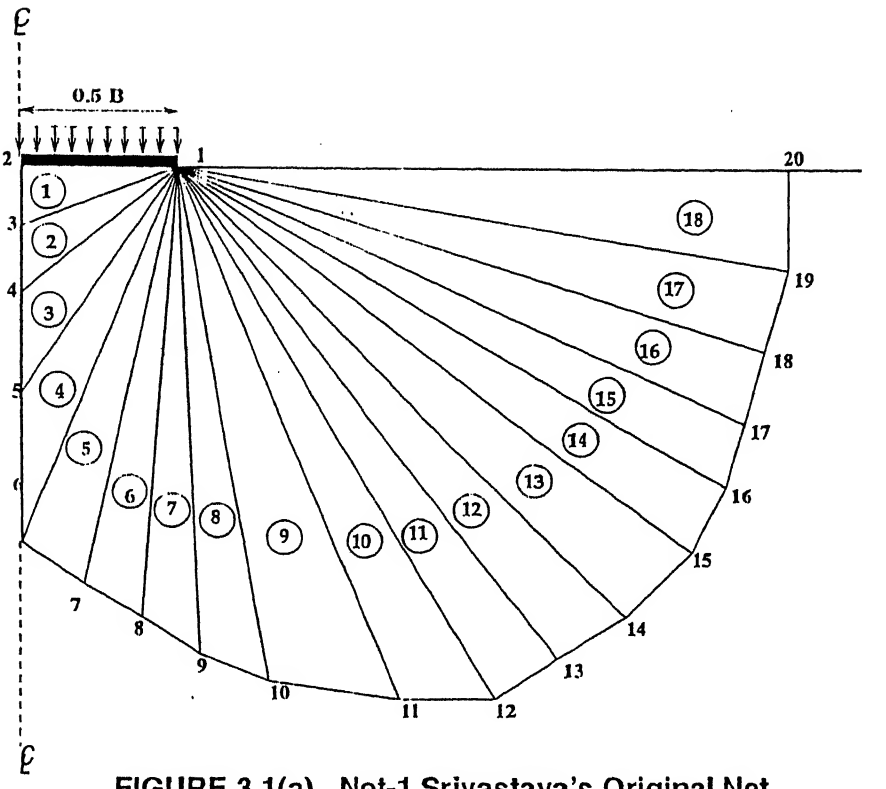

FIGURE 3.1(a) Net-1 Srivastava's Original Net

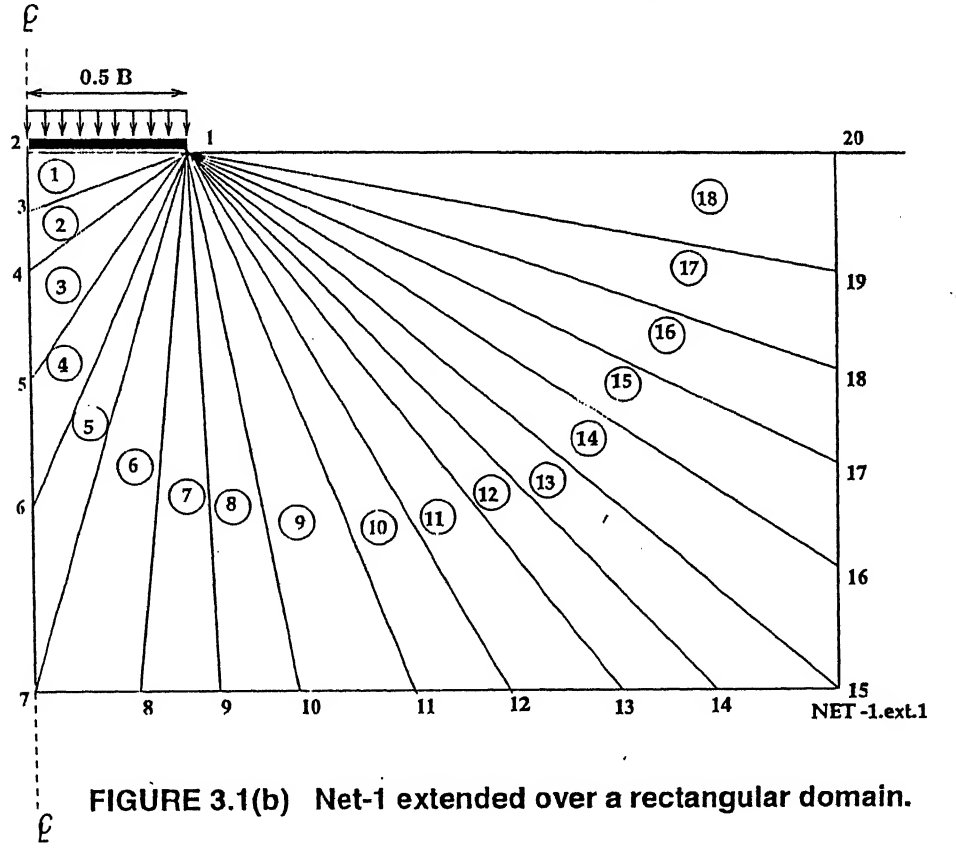

FIGURE 3.1(b) Net-1 extended over a rectangular domain.

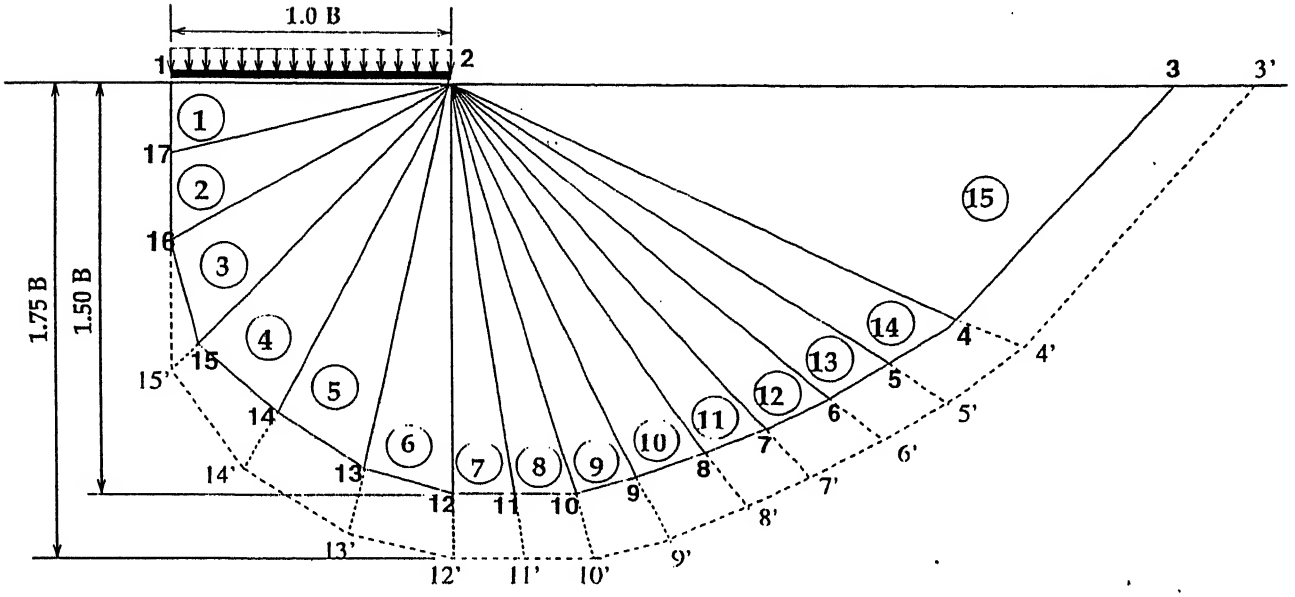

FIGURE 3.2(a) Net-2 for strip footing on homogeneous cohesive soil profile.

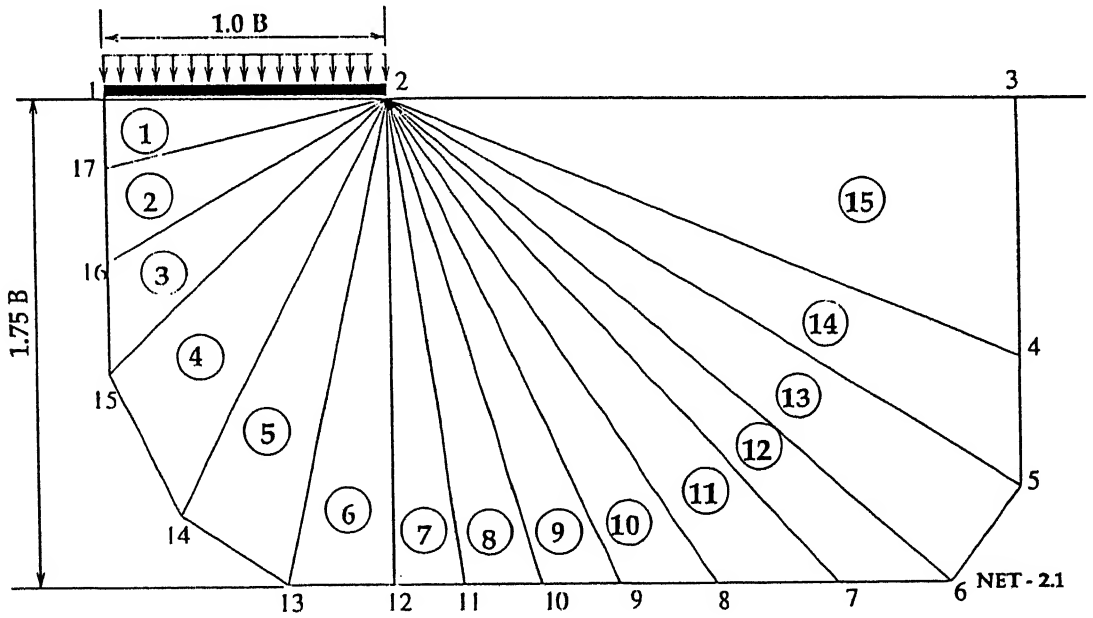

FIGURE 3.2(b) Extended Net-2 for strip footing on homogeneous cohesive soil

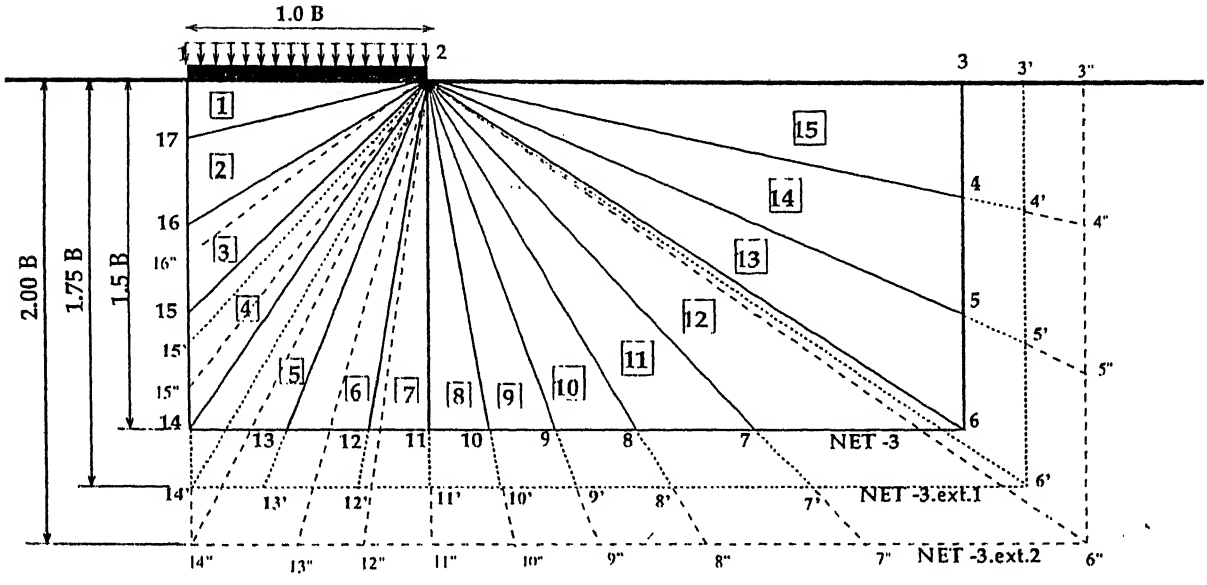

FIGURE 3.3(a) Net-3 for strip footing on homogenous cohesive soil.

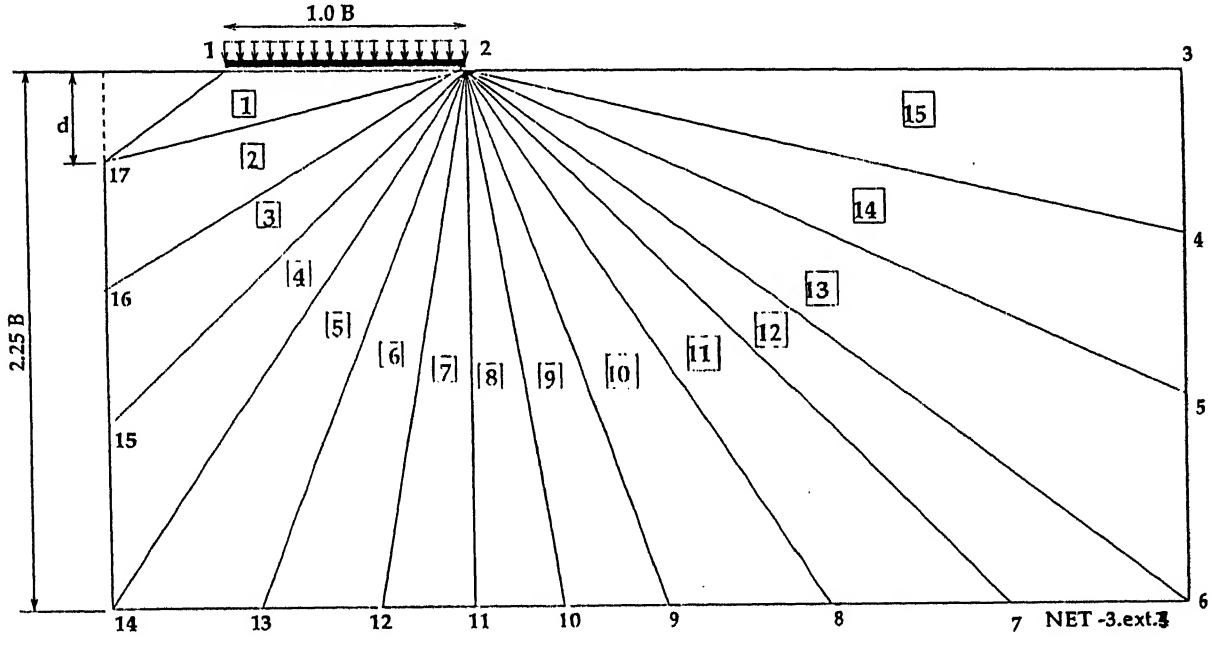

FIGURE 3.3(a) Extended Net-3 for strip footing on homogenous cohesive soil.

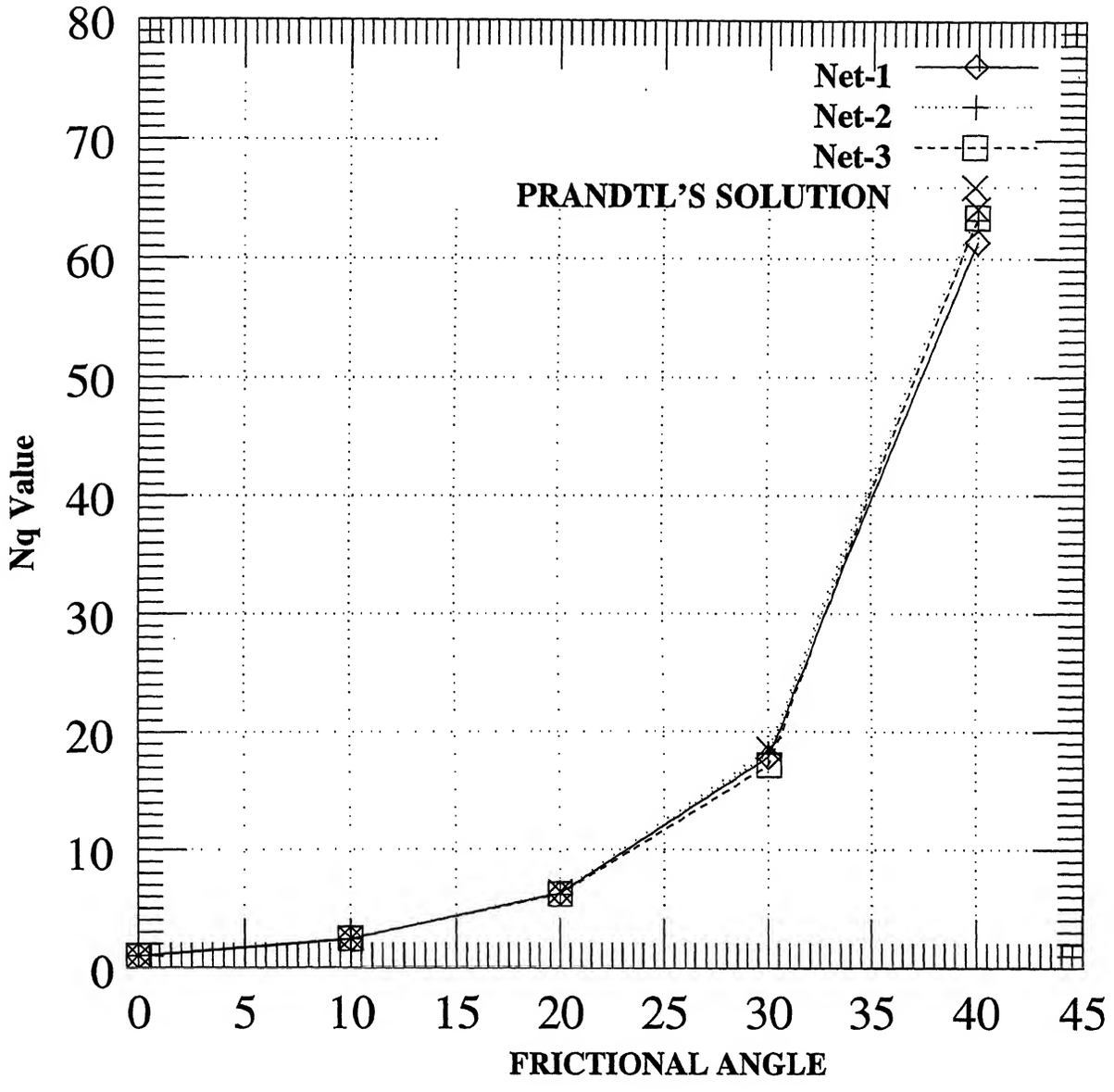

FIGURE 3.4 Nq VALUES Vs FRICTIONAL ANGLE

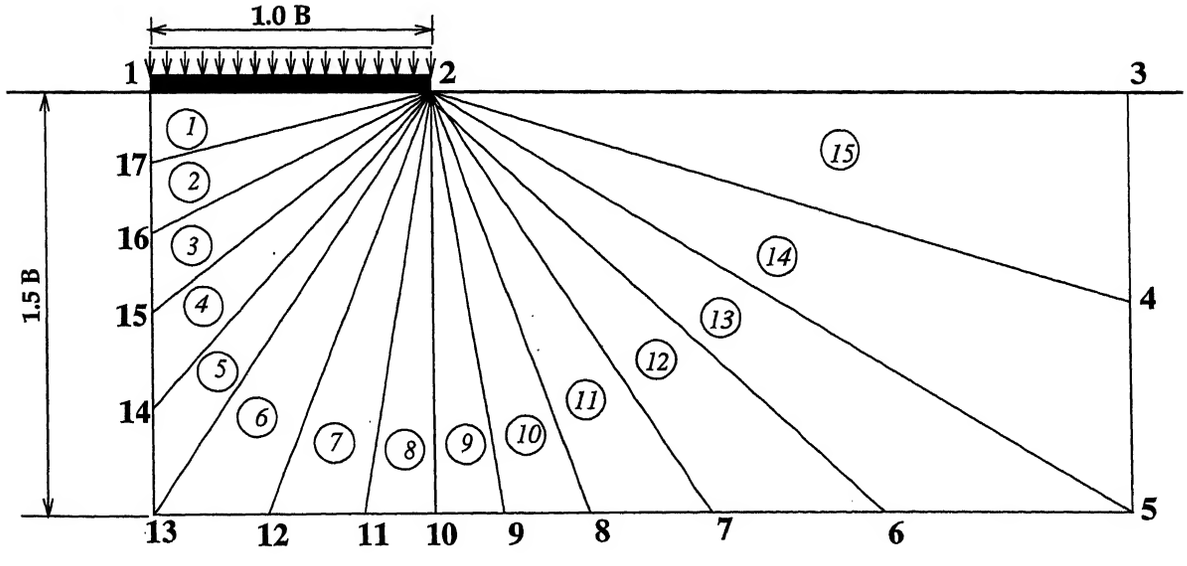

FIGURE 3.5 *Net used for Cohesive Frictional soils.*

Chapter 4

Lower bound bearing capacity of surface strip footing on two layered horizontal soil deposits.

4.1 Introduction

Some attempt to find a true lower bound solution were made by Srivastava (1993). However his studies were for limited depth of the upper layer and the obtained results were compared with only limit equilibrium solutions and experimental values. No comparison was made with any upper bound solution. As such there is some need to do that. In this study an effort has been made in that direction. In addition an attempt has been made to develop generalized mesh pattern for such an analysis.

4.2 The Problem

Fig 4.1 shows a smooth strip footing of width B lying on the surface of a fully saturated soil layer of thickness H having undrained shear strength parameter C_1, overlying another soil stratum having undrained shear strength C_2. The objective is to find a generalized mesh pattern for this problem and to determine the bearing

capacity of the strip footings for the different possible H/B ratios and compare them with available solutions.

The zone under consideration is divided into a number of elements and the nodal points, elements and element sides are numbered in some arbitrary manner. The various meshes used are shown in Fig 4.2 and will be discussed in detail in the following sections.

In order to find the lower bound solution of the layered deposits two types of boundary conditions were adopted. These are presented separately as case-1 and case-2 as follows:

Case-1 : Normal and shear stress discontinuity at the interface. In addition a no slip constraint at the interface was imposed in the form of $\tau_{i,j} \leq min(C_1, C_2)$ where i and j refer to the node points lying on the interface. To allow for this element sides and nodes lying on the layer interface have been marked differently (refer Fig 4.2(a)).

Case-2 : Normal and shear stress continuity at the layer interface: Here also the boundary condition, that the shear stresses at the interface must satisfy the no-slip condition. $\tau_{i,j} \leq min(C_1, C_2)$

The above two cases were taken up to investigate the effect of the two possible boundary conditions at the layer interface on the lower bound bearing capacity. The study was kept confined to a single C_1/C_2 ratio in order to study the various aspects of the lower bound solutions. As, in nature, the occurrence of stiff clay layer over weak clay layer is more common, in this study the undrained shear strength (C_1) of the upper layer has been taken as 65 kPa and the same for the lower layer (C_2) has been taken as 20 kPa.

4.3 The objective Function

The objective function is -$(\sigma_{1,2} + \sigma_{2,1})$ for all meshes shown in Fig 4.2 and Fig 4.3. Bearing capacity q_f is equal to half of the absolute value of the objective function value.

4.4 Stress discontinuity allowed at the interface

4.4.1 The boundary conditions

The boundary conditions for the meshes shown in Fig 4.2 are :

For Net-1 (refer Fig 4.2(a)) and Net-2 (refer Fig 4.2(b))

$$\sigma_{2,3} = \sigma_{3,2} = \sigma_{3,4} = \sigma_{4,3} = \sigma_{4,5} = \sigma_{5,4} = \sigma_{5,6} = \sigma_{6,5} = 0.0 \qquad (\textit{boundary condition})$$

$$\tau_{2,3} = \tau_{3,2} = \tau_{3,4} = \tau_{4,3} = \tau_{4,5} = \tau_{5,4} = \tau_{5,6} = \tau_{6,5} = 0.0 \qquad (\textit{boundary condition})$$

$$\tau_{1,2} = \tau_{2,1} = 0.0 \qquad (\textit{smooth footing})$$

$$\textit{and} \quad \tau_{1.12} = \tau_{12,1} = \tau_{13,24} = \tau_{24,13} = 0.0 \qquad (\textit{symmetry condition})$$

For Net-3, Net-3.ext.1 and Net-3.ext.2 (refer Fig 4.2(c))

$$\sigma_{2,3} = \sigma_{3,2} = \sigma_{3,4} = \sigma_{4,3} = \sigma_{4,5} = \sigma_{5,4} = 0.0$$

$$\sigma_{5,6} = \sigma_{6,5} = \sigma_{6,7} = \sigma_{7,6} = 0.0 \qquad (\textit{boundary condition})$$

$$\tau_{2,3} = \tau_{3,2} = \tau_{3,4} = \tau_{4,3} = \tau_{4,5} = \tau_{5,4} = 0.0$$

$$\tau_{5,6} = \tau_{6,5} = \tau_{6,7} = \tau_{7,6} = 0.0 \qquad (\textit{boundary condition})$$

$$\tau_{1,2} = \tau_{2,1} = 0.0 \qquad (\textit{smooth footing})$$

$$\textit{and} \quad \tau_{1,14} = \tau_{14,1} = \tau_{14,28} = \tau_{28,14} = 0.0 \qquad (\textit{symmetry condition})$$

For Net-4 (refer Fig 4.2(d))

$$\sigma_{2,3} = \sigma_{3,2} = 0.0 \qquad (\textit{boundary condition})$$

$$\tau_{2,3} = \tau_{3,2} = 0.0 \qquad (\textit{boundary condition})$$

$$\tau_{1,2} = \tau_{2,1} = 0.0 \qquad (\textit{smooth footing})$$

$$\textit{and} \quad \tau_{1,6} = \tau_{6,1} = \tau_{7,20} = \tau_{20,7} = \tau_{18,19} = \tau_{19,18} = 0.0$$

$$\tau_{19,20} = \tau_{20,19} = 0.0 \qquad (\textit{symmetry condition})$$

For Net-5 (refer Fig 4.2(e))

$$\sigma_{2,3} = \sigma_{3,2} = 0.0 \qquad (boundary \quad condition)$$

$$\tau_{2,3} = \tau_{3,2} = 0.0 \qquad (boundary \quad condition)$$

$$\tau_{1,2} = \tau_{2,1} = 0.0 \qquad (smooth \quad footing)$$

4.4.2 Results and discussions

The lower bound bearing capacity solutions were obtained on DEC OSF/ 1 computer system. The results obtained are presented for different H/B values as follows:

i) H/B = 0.25

A mesh pattern as indicated by Fig 4.2(a), Net-1, with 20 elements was taken up. Only half of the footing was considered and the chosen mesh was symmetric about the central line. The mesh pattern as can be seen from the Fig 4.2(a) is very simple and no concept of failure mechanism is involved.

The lower bound bearing capacity value obtained was 151.27 kPa, which was 6.25% less than that of the upper bound solution 161.36 kPa (Florkiewicz, 1988) and 14.75% more than that of experimental value of 131.82 kPa (Hanna and Meyerhof, 1978) for the same case.

Upon extension of the net both horizontally as well as vertically (Fig 4.2(a)) the obtained bearing capacity value (151.57 kPa) varied from the one obtained by the original mesh , by only 0.198% , which means the stress field is extensible and the predicted value is the true lower bound. So for this the critical solution will lie within a small range 151.57 kPa $\leq q_f \leq$ 161.36 kPa. The complete stress field along with stress-strength ratios at different nodal points for all the elements in Net-1 is presented in Table 4.1.

ii) H/B = 0.5

For this case a similar net as used for the previous case (H/B = 0.25) was taken up. First a 20 element net as shown in Fig 4.2(b) , similar to Net-1 but having a different set of co-ordinates was taken up to get the bearing capacity.

The lower bound value of bearing capacity obtained was 198.508 kPa . It is only 1.308% less than the upper bound solution, 201.14 kPa, of Florkiewicz (1988) and 21.14% more than that of Hanna and Meyerhof's (1978) experimental value (163.64 kPa). Here also the predicted lower bound solution is very close to the upper bound solution and this fact bounds the true critical load within a narrow range of (198.508 kPa and 201.14 kPa).

It is to be noted that the theoretically predicted values of the critical load by both the upper and lower bound approach of limit analysis are on the higher side of the experimental value. The experimental value is in fact an upper bound value as it is the observed collapse load. The lower bound solution is therefore expected to be lower than the experimentally observed value in contrary to the observation made in this study. If the allowance for experimental error of the order of 20% (very common) and an error of the order of 5% to 10% is made in the theoretical modeling of the problem, the discrepancy of the order of 20% in the predicted value is not very unlikely to occur.

Extension of the same mesh gave a result (198.425 kPa) differing only by 0.042% from the first solution . Studies regarding the extensibility of the stress field was under taken by adding four extra elements as shown in Fig 4.2.(c), Net-3, by dotted lines and in this case the bearing capacity value (196.154 kPa) varied only by 1.2% from the lower bound solution obtained by Net-2. The Net-3 was also extended vertically (Net-3,ext.1) and subsequently both vertically and horizontally (Net-3,ext.2) and bearing capacity values are 198.448 kPa and 197.983 kPa respectively, which are marginally different from the obtained value of the first solution 198.508 kPa (Net-2).

So every possible type of extensibility of stress field was ascertained and the obtained solutions varied from the upper bound solution as reported by Florkiewicz (1988) by only a maximum of 2.479% . So the solution may be considered to be a

true lower bound. The stress field associated with Net-2 is presented in Table 4.2 along with the stress-strength ratios at the various nodal points for all the element.

iii) H/B = 0.75

The mesh (Fig 4.2(b)) when applied for a H/B ratio of 0.75, did not provide good lower bound results and therefore a new mesh had to be tried out.The mesh pattern shown in Fig 4.2(d), Net-4 was tried. The idea behind this mesh pattern is that when the stronger upper layer is moderately large, its function may be only that of distribution of load to the lower layer in contrast to the action in the previous cases (H/B = 0.25 and 0.5) where in there is a possibility of a punching failure in the upper strata itself. Even though in finding the lower bound solution the failure state is not implied some idea of possible failure mechanism is generally of some help.

With this mesh the obtained lower bound bearing capacity value for H/B = 0.75 was 224.14 kPa. The value is just 5.17% less than the upper bound and 16.79% more than the experimental value. With the extended mesh (i.e. lower extent of mesh extended to 1.75 times the width of the footing, Net-4.ext.1) the obtained lower bound bearing capacity , (224.092 kPa) differed by 0.05% from the result (224.143 kPa) obtained by the original mesh (Net-4). So it can be concluded that the stress field is extensible. In Table 4.3, the complete stress field associated with Net-4 has been presented along with the stress-strength ratios at different nodal points for all the elements.

The same mesh (Net-4) was used for H/B = 0.5 and a lower bound solution of 178.87 kPa was obtained. This is less than the value obtained from Net-2 for the same case. This means that the Net-4 mesh pattern gives a non optimal lower bound solution for H/B = 0.5. When the H/B ratio was increased further, the value of lower bound solution obtained was again lesser than that obtained for this case (i.e. H/B =0.75) implying that similar to the case of H/B = 0.5 this mesh too produced non optimal lower bound solution for meshes with H/B ratio greater than 0.75.

Lower bound solution consistent with already obtained values for H/B=0.25 and 0.5, upper bound solution and experimental values could not be obtained for $0.75 \leq H/B \leq 1.5$.

iv) H/B =1.5

Many other types of nets were tried out to get lower bound bearing capacity solutions for H/B beyond 0.75 . After prolonged experimentation with various types of mesh patterns, unlike the previous cases an asymmetric mesh pattern (Net-5) Fig 4.2 (e), considering the whole footing width, comprising of 27 elements (Fig 4.2(e)), Net-5 was taken up.

The obtained lower bound bearing capacity was 322.45 kPa and it was only 4.135% less than the corresponding upper bound solution (336.36 kPa), but 19.29% higher than the experimental value (270.30 kPa) of Hanna and Meyerhof (1988). When the net was extended as indicated by Fig 4.2(e) the values obtained were 330.056 kPa and 329.01 kPa which were only 1.87% and 2.19% less than the upper bound solution of Florkiewicz (1988) but the difference with each other being only 0.35%. An extra element as indicated in Fig-4.2(e) was introduced and with that 28 element mesh the lower bound solution obtained was 325.20 kPa, which was 3.32% less than the upper bound solution. So for all practical purposes the stress field associated with the adopted mesh may be considered to be extensible.

The stress field and the stress-strength ratios at the different nodal points for all the elements associated with the Net-5 are presented in Table 4.4. It can seen from the Table 4.4 that the obtained stress field is excellent, as most of the stress-strength ratios are very close to unity thus signifying the limiting equilibrium state.

The same mesh (Net-5) was used for H/B ratio 1.75 and 2.0. The obtained lower bound solutions were 329.563 kPa and 329.80 kPa respectively which were 2.02% and 1.95% less than the corresponding upper bound solutions and 11.94% and 6.39% more than the corresponding experimental values.

The values of lower bound bearing capacity for the H/B = 1.5, 1.75 and 2.0 varied from each other by a maximum of 0.149% which was almost negligible. This indicates that the effect of layering at a depth beyond 1.5 times the footing width is not significant. The upper layer controls the bearing capacity if the depth of upper layer exceeds 1.5 times the footing width.

It can also be concluded that the Net-5, is capable of providing lower bound

solution for H/B =1.5 and beyond.

It has been observed that the best result is achieved when the horizontal extent of the net is 3.5 times the width of the footing and the vertical extent is 2.25 times the width of the footing for H/B ratio of 1.5.

All the lower bound bearing capacity solutions obtained by various mesh patterns shown in Fig 4.2, have been presented in a tabulated form in the Table 4.5 and also in a graphical form in Figure 4.4. In Table 4.1 all the relevant values reported by Florkiewicz (1988), Hanna and Meyerhof (1978) and Button (1953) are also presented for ready reference and comparison.

In addition the bearing capacity values were also computed by treating the medium as an equivalent homogeneous medium. The equivalent undrained shear strength values were computed by using the relation.

$$C_{avg.} = \frac{(C_1H_1 + C_2H_2)}{(H_1 + H_2)}$$

The bearing capacity values were computed by multiplying the $C_{avg.}$ value for various H/B cases with the N_c value of (5.05) obtained from the lower bound approach. These values shows good agreement with the experimental results (refer Fig 4.4)

4.5 Normal and shear stress continuity at layer interface

Unlike the previous case, where for every other H/B ratio, a different mesh had to be used for getting a lower bound solution, here the same mesh (Fig 4.3) was used for getting lower bound bearing capacity solution for all different H/B ratio.

4.5.1 The boundary conditions

The boundary conditions for the meshes shown in Fig 4.3 are :
For Net-5 (refer Fig 4.2(e))

$$\sigma_{2,3} = \sigma_{3,2} = 0.0 \qquad (boundary \quad condition)$$

$$\tau_{2,3} = \tau_{3,2} = 0.0 \qquad (boundary \quad condition)$$

$$\tau_{1,2} = \tau_{2,1} = 0.0 \qquad (smooth \quad footing)$$

4.5.2 Result and Discussions

The results obtained are presented in a tabulated form in Table 4.5 along with other solutions obtained for all other cases.

It can be observed from the results presented in the Table 4.5 that for the case-2 the predicted solutions are always substantially lower than that of case-1. However, here an increasing trend in the bearing capacity values is noticed as H/B ratio increases. But the lower bound solutions obtained, by this mesh pattern and boundary conditions imposed at the layer interface, is not the maximum possible bearing capacity. Further studies are needed to be conducted with the same boundary conditions but different mesh patterns. The lower bound solutions obtained with the chosen mesh pattern gave very low values (even lower that of 100.96 kPa obtained by treating the top stiff layer as non-existent) indicating the non-optimality of the solution. So further studies are needed in order to find the reasons for the same.

4.6 Conclusions:

Based on the results and discussions as presented the following conclusions can be drawn:

1. A unified mesh pattern for varying H/B ratio could not be developed and more studies are required to find the reasons for the same.

2. Some success has been attained in developing a general mesh pattern (with discontinuity of normal and shear stress at the layer interface) for $H/B \leq 0.5$, $H/B = 0.75$ and $H/B \geq 1.5$. However, a gap, $0.75 < H/B < 1.5$ remained where solution could not be achieved. Allowing for normal and shear stress continuity at the layer interface, the gap is $0 < H/B < 1.0$ where again solutions could not be found.

3. Solutions obtained with the imposition of normal stress and shear stress continuity at the layer interface are very very low in comparison to the values obtained where in normal and shear stress discontinuity has been allowed with a no-slip condition at the interface.

4. Solutions obtained with the imposition of stress discontinuity are in close agreement with the upper bound solutions and the experimental results.So, for obtaining a realistic lower bound solutions the condition of normal stress discontinuity with a no-slip condition must be imposed at the layer interface.

5. The obtained statically admissible stress fields for the various mesh patterns considered were found to be extensible. As such the solutions obtained can be considered to be the true lower bounds.

6. When the medium is treated as an equivalent homogeneous medium the approximate lower bound bearing capacity values are found to be in close agreement with the experimental values of Hanna and Meyerhof.

Table 4.1

Stress Field and Stress-Strength Ratios at the

Nodal Points (for H/B ratio 0.25)

Net-1

Element No.	Nodal Point	σ_x	σ_z	τ_{zx}	Stress Strength ratio
1	2	0.254441E+02	0.124466E+02	0.953674E-06	0.999617E+00
1	1	0.254441E+02	0.178666E+02	0.381624E-05	0.339761E+00
1	12	0.486820E+01	0.178671E+02	0.381624E-05	0.999831E+00
2	2	0.652866E+01	0.190024E+02	0.182687E+01	0.999663E+00
2	12	0.180825E+02	0.962802E+01	0.493549E+01	0.999494E+00
2	11	0.983447E+01	0.203221E+02	0.229715E+01	0.775723E+00
3	2	0.652866E+01	-0.194703E+00	0.194702E+00	0.268374E+00
3	11	0.983447E+01	0.546815E+01	0.611936E+01	0.999118E+00
3	10	0.352041E+01	0.138855E+01	0.457028E+00	0.318362E-01
4	2	0.672337E+01	0.000000E+00	0.000000E+00	0.267477E+00
4	10	0.304187E+01	0.524522E-03	0.476262E+00	0.601010E-01
4	3	0.719963E+01	0.000000E+00	0.476080E-06	0.306714E+00
5	3	0.719962E+01	0.359981E+01	0.359981E+01	0.383392E+00
5	10	0.304187E+01	0.423523E+01	0.173763E+01	0.798909E-01
5	9	0.490405E+01	0.192951E+01	0.110274E+01	0.811362E-01
6	3	0.359981E+01	0.000000E+00	0.283080E-09	0.766784E-01
6	9	0.263230E+01	0.524046E-03	0.997627E+00	0.645403E-01
6	4	0.459744E+01	0.000000E+00	0.239175E-06	0.125068E+00
7	4	0.459744E+01	0.229872E+01	0.229872E+01	0.156335E+00
7	9	0.263231E+01	0.183394E+01	0.646048E+00	0.136503E-01
7	8	0.428498E+01	0.105081E+01	0.111135E+01	0.911256E-01
8	4	0.229872E+01	0.000000E+00	0.238419E-06	0.312670E-01
8	8	0.296323E+01	0.524642E-03	0.746644E-01	0.520706E-01
8	5	0.237339E+01	0.000000E+00	0.239117E-06	0.333311E-01
9	5	0.237338E+01	0.228210E+00	0.593346E+00	0.355622E-01
9	8	0.296323E+01	0.283207E+00	0.616990E+00	0.515103E-01
9	7	0.291595E+01	0.855861E+00	0.508045E+00	0.312212E-01
10	5	0.912841E+00	0.000000E+00	0.936166E-08	0.493064E-02
10	7	0.947468E+00	0.524969E-03	0.839412E+00	0.219831E-01
10	6	0.259167E+01	0.000000E+00	0.240048E-06	0.397440E-01

contd. on next page

Table 4.1

Element No.	Nodal Point	σ_x	σ_z	τ_{zx}	Stress Strength ratio
11	19	0.251081E+00	0.383580E+01	0.465128E+00	0.857225E+00
11	18	0.336118E+01	0.398963E+01	0.177057E+01	0.808413E+00
11	17	0.283900E+01	0.311088E+01	0.170804E+01	0.733967E+00
12	19	0.156575E+00	0.101522E+01	0.217121E+00	0.578643E-01
12	17	0.961744E+00	0.337373E+01	0.585969E+00	0.449445E+00
12	20	0.243508E+00	0.299744E+01	0.368637E+00	0.507983E+00
13	20	0.243508E+00	0.313381E+01	0.240133E+00	0.536531E+00
13	17	0.961744E+00	0.370961E+01	0.121986E+01	0.843937E+00
13	16	0.765799E+00	0.350606E+01	0.110420E+01	0.774131E+00
14	20	0.405495E+00	0.887960E+00	0.420518E+00	0.587571E-01
14	16	0.276586E+00	0.358802E+01	0.110633E+00	0.688411E+00
14	21	0.415301E+00	0.117991E+01	0.616047E-01	0.374878E-01
15	21	0.415301E+00	0.342845E+01	0.976648E+00	0.805904E+00
15	16	0.276585E+00	0.364900E+01	0.696426E+00	0.832075E+00
15	15	0.332630E+00	0.366234E+01	0.651818E+00	0.799152E+00
16	21	0.457473E+00	0.749379E+00	0.814172E+00	0.171045E+00
16	15	0.116881E+00	0.378036E+01	0.124250E+00	0.842674E+00
16	22	0.472228E+00	0.702115E+00	0.198025E+00	0.131064E-01
17	22	0.472229E+00	0.287864E+01	0.137860E+01	0.837057E+00
17	15	0.116882E+00	0.341975E+01	0.712576E+00	0.808750E+00
17	14	0.250086E+00	0.348369E+01	0.603854E+00	0.744671E+00
18	22	0.429330E+00	0.976889E+00	0.108118E+01	0.310974E+00
18	14	0.841936E-01	0.368224E+01	0.208978E+00	0.820037E+00
18	23	0.488897E+00	0.812924E+00	0.506812E+00	0.707766E-01
19	23	0.488897E+00	0.356522E+01	0.111793E+01	0.903929E+00
19	14	0.841937E-01	0.362272E+01	0.482846E+00	0.840860E+00
19	13	0.338229E+00	0.235111E+01	0.458845E+00	0.305866E+00
20	23	0.271397E+00	0.145915E+01	0.424845E+00	0.133295E+00
20	13	-0.145799E-02	0.217993E+01	0.689179E-07	0.297403E+00
20	24	0.271397E+00	0.112032E+01	0.550062E-08	0.450416E-01

Table 4.2

Stress Field and Stress-Strength Ratios at the Nodal Points (for H/B ratio 0.50)

Net-2

Element No.	Nodal Point	σ_x	σ_z	τ_{zx}	Stress Strength ratio
1	2	0.713423E+01	0.195682E+02	0.953674E-06	0.914814E+00
1	1	0.713423E+01	0.201334E+02	0.151340E-08	0.999876E+00
1	12	0.782503E+01	0.201345E+02	0.151340E-08	0.896582E+00
2	2	0.523836E+01	0.176723E+02	0.189587E+01	0.999887E+00
2	12	0.541012E+01	0.173005E+02	0.262441E+01	0.999600E+00
2	11	0.729648E+01	0.202883E+02	0.951648E-02	0.998740E+00
3	2	0.523836E+01	0.141401E+02	0.451505E+01	0.951383E+00
3	11	0.729648E+01	0.133643E+02	0.574690E+01	0.999562E+00
3	10	0.668055E+01	0.109676E+02	0.613531E+01	0.999686E+00
4	2	0.425833E+01	0.000000E+00	0.953674E-06	0.107298E+00
4	10	0.229037E+01	0.104523E-02	0.996515E+00	0.545157E-01
4	3	0.475659E+01	0.000000E+00	0.143124E-05	0.133876E+00
5	3	0.475659E+01	0.135903E+02	0.475659E+01	0.997243E+00
5	10	0.229037E+01	0.102188E+02	0.211593E+01	0.477923E+00
5	9	0.361070E+01	0.910094E+01	0.380217E+01	0.520525E+00
6	3	0.339756E+01	0.000000E+00	0.593468E-06	0.683043E-01
6	9	0.523397E+00	0.104618E-02	0.156011E+01	0.592225E-01
6	4	0.417761E+01	0.000000E+00	0.829459E-09	0.103269E+00
7	4	0.417762E+01	0.119360E+02	0.417762E+01	0.769248E+00
7	9	0.523398E+00	0.844286E+01	0.181362E+00	0.371891E+00
7	8	0.252152E+01	0.336904E+01	0.192848E+01	0.922746E-01
8	4	0.298401E+01	0.000000E+00	0.000000E+00	0.526882E-01
8	8	0.133457E+01	0.105381E-02	0.100470E+00	0.107613E-01
8	5	0.303424E+01	0.000000E+00	0.771252E-09	0.544771E-01
9	5	0.303424E+01	0.151712E+01	0.151712E+01	0.680963E-01
9	8	0.133457E+01	0.179216E+01	0.850095E+00	0.183434E-01
9	7	0.200160E+01	0.137875E+01	0.576107E+00	0.101511E-01
10	5	0.151712E+01	0.000000E+00	0.101335E-07	0.136193E-01
10	7	0.386892E+00	0.104988E-02	0.920097E+00	0.209183E-01
10	6	0.243722E+01	0.000000E+00	0.145519E-08	0.351482E-01

contd. on next page

Table 4.2

Element No.	Nodal Point	σ_x	σ_z	τ_{zx}	Stress Strength ratio
11	19	0.146021E+00	0.389047E+01	0.361688E+00	0.909012E+00
11	18	0.424654E+01	0.422258E+01	0.188169E+01	0.885229E+00
11	17	0.363854E+01	0.271051E+01	0.174785E+01	0.817572E+00
12	19	0.423650E-01	0.107408E+01	0.331161E+00	0.939439E-01
12	17	0.126004E+01	0.451928E+01	0.863510E+00	0.850326E+00
12	20	0.116802E+00	0.365613E+01	0.677418E+00	0.897653E+00
13	20	0.116802E+00	0.325193E+01	0.385414E+00	0.651450E+00
13	17	0.126004E+01	0.386766E+01	0.133390E+01	0.869798E+00
13	16	0.916181E+00	0.372788E+01	0.121025E+01	0.860278E+00
14	20	0.395994E+00	0.976837E+00	0.850545E-01	0.228947E-01
14	16	0.324108E+00	0.383953E+01	0.258769E+00	0.789126E+00
14	21	0.369183E+00	0.145264E+01	0.392824E+00	0.111945E+00
15	21	0.369183E+00	0.373869E+01	0.530134E+00	0.779861E+00
15	16	0.324108E+00	0.388366E+01	0.589063E+00	0.878648E+00
15	15	0.312322E+00	0.389411E+01	0.559570E+00	0.880106E+00
16	21	0.523116E+00	0.509848E+00	0.592082E+00	0.876513E-01
16	15	0.103273E+00	0.378445E+01	0.259818E-01	0.847112E+00
16	22	0.508354E+00	0.587397E+00	0.478295E-01	0.962397E-03
17	22	0.508354E+00	0.319945E+01	0.122306E+01	0.826590E+00
17	15	0.103273E+00	0.359539E+01	0.621731E+00	0.858819E+00
17	14	0.223538E+00	0.373020E+01	0.542042E+00	0.841995E+00
18	22	0.553849E+00	0.941998E+00	0.111105E+01	0.318024E+00
18	14	0.794233E-01	0.379920E+01	0.188657E+00	0.873693E+00
18	23	0.615403E+00	0.728586E+00	0.496427E+00	0.624106E-01
19	23	0.615403E+00	0.351894E+01	0.126568E+01	0.927396E+00
19	14	0.794234E-01	0.365047E+01	0.511261E+00	0.862369E+00
19	13	0.381192E+00	0.293697E+01	0.457650E+00	0.460611E+00
20	23	0.519435E+00	0.216835E+01	0.875604E+00	0.361603E+00
20	13	-0.306502E-01	0.322273E+01	0.241853E-07	0.661530E+00
20	24	0.519435E+00	0.103622E+01	0.128377E-06	0.166917E-01

Table 4.3

Stress Field and Stress-Strength Ratios at the Nodal Points (for H/B ratio 0.75)

Net-4

Element No.	Nodal Point	σ_x	σ_z	τ_{zx}	Stress Strength ratio
1	2	0.101887E+02	0.231880E+02	0.476837E-06	0.999899E+00
1	1	0.101887E+02	0.216359E+02	0.190886E-05	0.775379E+00
1	6	0.122766E+02	0.216375E+02	0.955188E-06	0.518495E+00
2	2	0.101279E+02	0.531561E+01	0.600307E+01	0.989972E+00
2	6	0.844401E+01	0.112072E+02	0.635122E+01	0.999923E+00
2	5	0.108749E+02	0.325725E+01	0.183454E+01	0.423020E+00
3	2	0.343732E+01	0.000000E+00	0.386100E-08	0.699122E-01
3	5	0.127908E+02	0.157511E-02	0.116468E+01	0.999945E+00
3	3	0.719743E+00	0.000000E+00	0.103551E-06	0.306527E-02
4	3	0.814924E+01	0.417909E+01	0.557212E+01	0.828143E+00
4	5	0.126974E+02	-0.509576E-01	0.123472E+01	0.997749E+00
4	4	0.238818E+01	0.348685E+01	0.215981E+01	0.117552E+00
5	8	0.378622E+01	0.705966E+00	0.103820E+01	0.862463E+00
5	10	0.442231E+01	0.107814E+01	0.823384E+00	0.868454E+00
5	9	0.420877E+01	0.105035E+01	0.929021E+00	0.839247E+00
6	8	0.334524E+01	0.939982E+00	0.145111E+01	0.888005E+00
6	11	0.322924E+01	0.145060E+01	0.169663E+01	0.917356E+00
6	10	0.335512E+01	0.159967E+01	0.173304E+01	0.943456E+00
7	8	0.310332E+01	0.169833E+01	0.186596E+01	0.993823E+00
7	12	0.287131E+01	0.188911E+01	0.192112E+01	0.982973E+00
7	11	0.285126E+01	0.201353E+01	0.193017E+01	0.975252E+00
8	8	0.196628E+01	0.205436E+01	0.133207E+01	0.444089E+00
8	13	0.158399E+01	0.298593E+01	0.182522E+01	0.955699E+00
8	12	0.130391E+01	0.348631E+01	0.164619E+01	0.975164E+00
9	8	0.112087E+01	0.210403E+01	0.327923E+00	0.872965E-01
9	14	0.959105E+00	0.164964E+01	0.810056E+00	0.193850E+00
9	13	0.758216E+00	0.378134E+01	0.100001E+01	0.821211E+00
10	8	0.112086E+01	0.187488E+01	0.792942E+00	0.192723E+00
10	15	0.119015E+01	0.841306E+00	0.638678E+00	0.109583E+00
10	14	0.959104E+00	0.126072E+01	0.330849E+00	0.330510E-01

contd. on next page

Table 4.3

Element No.	Nodal Point	σ_x	σ_z	τ_{zx}	Stress Strength ratio
11	8	0.176431E+01	0.784093E+00	0.116369E+01	0.398594E+00
11	16	0.170982E+01	0.118741E+01	0.114450E+01	0.344526E+00
11	15	0.160461E+01	0.889902E+00	0.106528E+01	0.315632E+00
12	8	0.272403E+01	0.119138E+01	0.181259E+01	0.968180E+00
12	17	0.264692E+01	0.205549E+01	0.191983E+01	0.943302E+00
12	16	0.257904E+01	0.175297E+01	0.184693E+01	0.895434E+00
13	8	0.142464E+01	0.731182E+00	0.103927E+01	0.300075E+00
13	18	0.593865E+00	0.431979E+00	0.582077E-07	0.163794E-02
13	17	0.178475E+00	0.640332E+00	0.610016E-07	0.133320E-01
14	8	0.259510E+00	0.239429E+00	0.191550E+00	0.919809E-02
14	19	0.234653E+01	-0.779093E-01	0.298023E-06	0.367369E+00
14	18	0.359874E+01	-0.488017E-01	0.417233E-06	0.831536E+00
15	8	0.106383E+01	0.420523E-01	0.102664E+00	0.678871E-01
15	20	0.213145E+01	-0.149532E+00	0.266824E-06	0.325181E+00
15	19	0.373288E+01	-0.164556E+00	0.311527E-06	0.949377E+00
16	8	0.247675E+01	-0.155922E-01	0.320239E+00	0.413875E+00
16	7	0.247675E+01	-0.100200E+00	0.356697E-06	0.415043E+00
16	20	0.375619E+00	-0.131974E+00	0.386499E-06	0.161032E-01

Table 4.4

Stress Field and Stress-Strength Ratios at the Nodal Points (for H/B ratio 1.5)

Net-5

Element No.	Nodal Point	σ_x	σ_z	τ_{zx}	Stress Strength ratio
1	2	0.204316E+02	0.330222E+02	0.231934E-02	0.938005E+00
1	1	0.200104E+02	0.330091E+02	0.255203E-02	0.999798E+00
1	17	0.200122E+02	0.330092E+02	0.102749E+00	0.999780E+00
2	2	0.199986E+02	0.329951E+02	0.110592E+00	0.999749E+00
2	17	0.200112E+02	0.330091E+02	0.102489E+00	0.999932E+00
2	16	0.199240E+02	0.329226E+02	0.759926E-01	0.999923E+00
3	2	0.205089E+02	0.331945E+02	0.208361E+00	0.953236E+00
3	16	0.199482E+02	0.329320E+02	0.911407E-01	0.997712E+00
3	15	0.203139E+02	0.332503E+02	0.529984E+00	0.996881E+00
4	2	0.190768E+02	0.317624E+02	0.122372E+01	0.987650E+00
4	15	0.193762E+02	0.323126E+02	0.407700E+00	0.994170E+00
4	14	0.182926E+02	0.306712E+02	0.164100E+01	0.970431E+00
5	2	0.173506E+02	0.278783E+02	0.381309E+01	0.999951E+00
5	14	0.172953E+02	0.284273E+02	0.313697E+01	0.966179E+00
5	13	0.168627E+02	0.267896E+02	0.407319E+01	0.975787E+00
6	2	0.166584E+02	0.231681E+02	0.561871E+01	0.997959E+00
6	13	0.164102E+02	0.237102E+02	0.525365E+01	0.968602E+00
6	12	0.162507E+02	0.217803E+02	0.587599E+01	0.998138E+00
7	2	0.165229E+02	0.182897E+02	0.643174E+01	0.997578E+00
7	12	0.161719E+02	0.189429E+02	0.634890E+01	0.999481E+00
7	11	0.161675E+02	0.176346E+02	0.645808E+01	0.999879E+00
8	2	0.165229E+02	0.146620E+02	0.643176E+01	0.999603E+00
8	11	0.161675E+02	0.152181E+02	0.645808E+01	0.992478E+00
8	10	0.161631E+02	0.136484E+02	0.636541E+01	0.996435E+00
9	2	0.164190E+02	0.109198E+02	0.580806E+01	0.977367E+00
9	10	0.160960E+02	0.112319E+02	0.596266E+01	0.981493E+00
9	9	0.160112E+02	0.966632E+01	0.563931E+01	0.990913E+00
10	2	0.155726E+02	0.462436E+01	0.349972E+01	0.999150E+00
10	9	0.154702E+02	0.564238E+01	0.416386E+01	0.981874E+00
10	8	0.149111E+02	0.379918E+01	0.318262E+01	0.970367E+00

contd. on next page

Table 4.4

Element No.	Nodal Point	σ_x	σ_z	τ_{zx}	Stress Strength ratio
11	2	0.141797E+02	0.149026E+01	0.141031E+01	0.999864E+00
11	8	0.139692E+02	0.167971E+01	0.176964E+01	0.967792E+00
11	7	0.135817E+02	0.117217E+01	0.136812E+01	0.955524E+00
12	2	0.126974E+02	0.794323E-02	0.719912E-01	0.952912E+00
12	7	0.133090E+02	0.899432E+00	0.109539E+01	0.939623E+00
12	6	0.117854E+02	0.405244E+00	0.155454E+00	0.766885E+00
13	2	0.124277E+02	-0.111917E+00	0.251785E+00	0.931922E+00
13	6	0.936354E+01	-0.671119E+00	0.145909E+01	0.646214E+00
13	5	0.121339E+02	-0.162061E+00	0.293069E+00	0.896659E+00
14	2	0.129943E+02	0.123521E-04	0.586273E-04	0.999125E+00
14	5	0.129279E+02	-0.523144E-02	0.597974E-01	0.989823E+00
14	4	0.129078E+02	-0.249541E-02	0.360839E-01	0.986271E+00
15	2	0.129941E+02	0.000000E+00	0.138224E-05	0.999087E+00
15	4	0.129583E+02	-0.894070E-07	0.473108E-01	0.993645E+00
15	3	0.127812E+02	0.000000E+00	0.178814E-05	0.966618E+00
16	27	0.188322E+01	0.585363E+01	0.215339E+00	0.996853E+00
16	26	0.291164E+01	0.686775E+01	0.291256E+00	0.999383E+00
16	25	0.236009E+01	0.580867E+01	0.336215E+00	0.771554E+00
17	27	0.188322E+01	0.300743E+01	0.726273E+00	0.210858E+00
17	25	0.236009E+01	0.391039E+01	0.183013E+01	0.987558E+00
17	24	0.162419E+01	0.476826E+01	0.122816E+01	0.994918E+00
18	28	0.417333E+00	0.387514E+01	0.118769E+00	0.750805E+00
18	27	0.173556E+01	0.238929E+01	0.409476E+00	0.686281E-01
18	24	0.232395E+01	0.340082E+01	0.129717E+01	0.493144E+00
19	28	0.422563E+00	0.419229E+01	0.192652E-01	0.888272E+00
19	24	0.196960E+01	0.522020E+01	0.104666E+01	0.934277E+00
19	23	0.195627E+01	0.586761E+01	0.414698E-01	0.956591E+00
20	28	0.422564E+00	0.227045E+01	0.371401E+00	0.247902E+00
20	23	0.195627E+01	0.360775E+01	0.178908E+01	0.970660E+00
20	22	0.138920E+01	0.303167E+01	0.125415E+01	0.561832E+00
21	28	0.557567E+00	0.902356E+00	0.266536E+00	0.251903E-01
21	22	0.812901E+00	0.868848E+00	0.101211E+00	0.275653E-02
21	29	0.650370E+00	0.663203E+00	0.195447E+00	0.956019E-02
22	29	0.379212E+00	0.437415E+01	0.163075E-01	0.997538E+00
22	22	0.466378E+00	0.441625E+01	0.297603E-01	0.975314E+00
22	21	0.454317E+00	0.440381E+01	0.198733E-01	0.975005E+00

contd. on next page

Table 4.4

Element No.	Nodal Point	σ_x	σ_z	τ_{zx}	Stress Strength ratio
23	29	0.379212E+00	0.343023E+01	0.552511E+00	0.658110E+00
23	21	0.454318E+00	0.412974E+01	0.663796E+00	0.954450E+00
23	20	0.417222E+00	0.134658E+01	0.430626E+00	0.100342E+00
24	29	0.532991E+00	0.199180E+01	0.543442E+00	0.206839E+00
24	20	0.417024E+00	0.112484E+01	0.393372E+00	0.699977E-01
24	30	0.712391E+00	0.576901E+00	0.736480E+00	0.136748E+00
25	30	0.402521E+00	0.423985E+01	0.300383E+00	0.942876E+00
25	20	0.145127E+00	0.407574E+01	0.677379E-01	0.966752E+00
25	19	0.175719E+00	0.386589E+01	0.229786E+00	0.864287E+00
26	30	0.402521E+00	0.405340E+01	0.764832E+00	0.979301E+00
26	19	0.175719E+00	0.389039E+01	0.487967E+00	0.921952E+00
26	18	0.332609E+00	0.336282E+01	0.580340E+00	0.658084E+00
27	30	0.836005E+00	0.406340E+01	0.115015E+01	0.981717E+00
27	18	0.393027E-01	0.357149E+01	0.380662E+00	0.815996E+00
27	31	0.144641E+01	0.411447E+01	0.145784E+01	0.976237E+00

Table 4.5

BEARING CAPACITY VALUES FOR VARIOUS H/B RATIO

H/B	Case-1 # (stress discont.)	Case-2 # (stress cont.)	Equivalent # Cohesion Case	Upper #+ bound Florkiewicz	Experimental Hanna Meyerhof +	Limit Equilibrium Button ++
0.00	100.960	100.960	100.960	101.00	101.00	--
0.25	151.570	??	129.406	161.36	131.82	--
0.50	198.508	??	157.813	201.14	163.64	162.500
0.75	224.140	??	186.220	236.36	190.91	--
1.00	??	132.160	214.650	270.45	218.18	207.187
1.25	??	171.472	243.031	304.54	249.56	--
1.50	330.056	197.719	271.440	336.36	270.32	--
1.75	329.563	220.990	299.843	336.36	294.40	--
2.00	329.800	229.170	328.250	336.36	310.04	284.375
2.25	--	247.900	--	336.36	329.27	--
2.50	--	265.990	--	336.36	336.36	--
2.75	--	271.235	--	336.36	336.36	--
3.00	--	275.25	--	336.36	336.36	357.500

present study, #+ 1988,

+ 1978, , ++ 1953

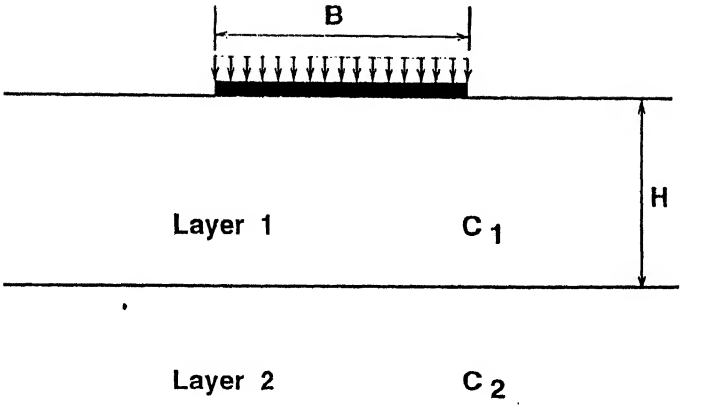

Fig. 4.1 Details of Surface Footing on Two Layered Soil Deposit.

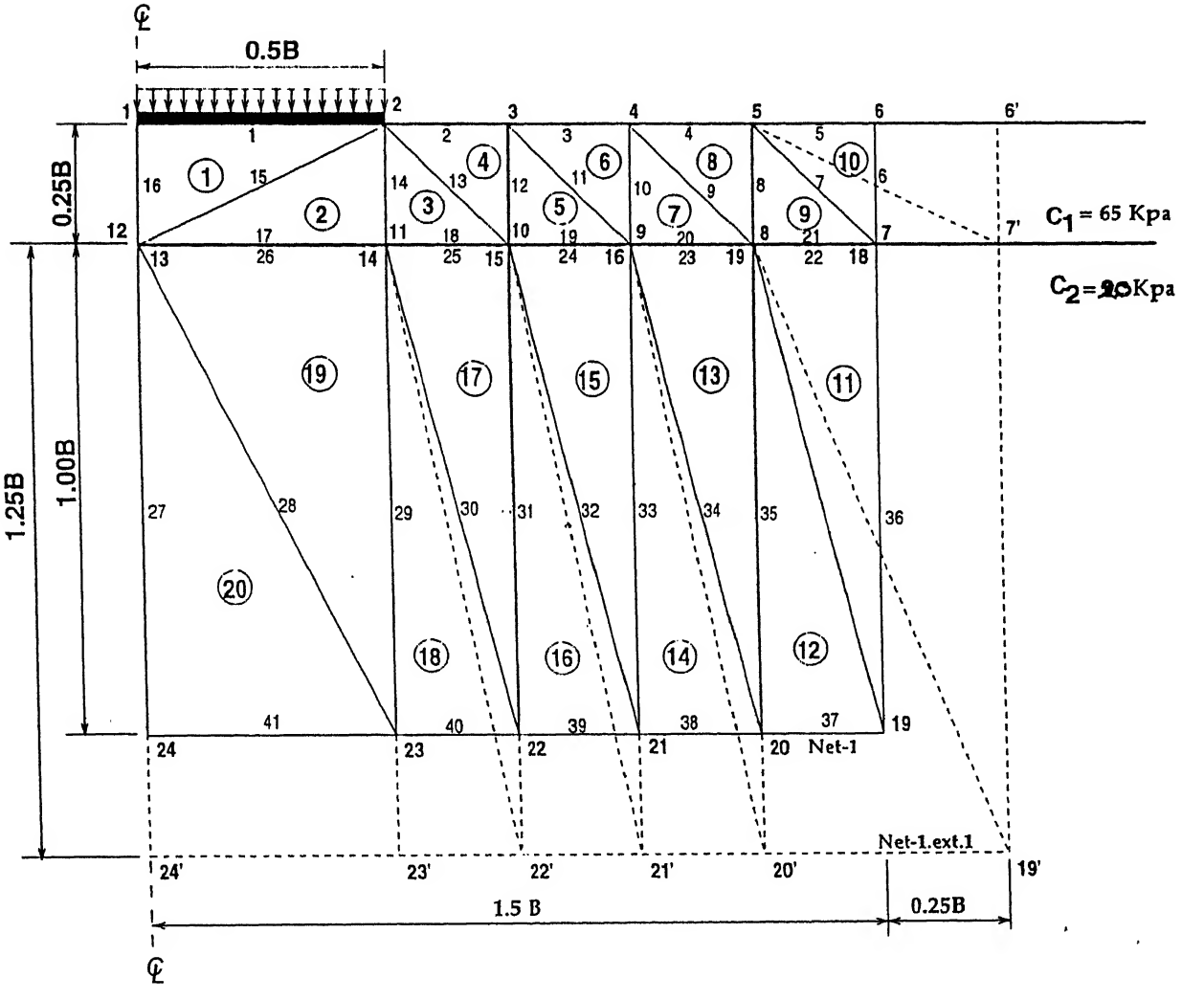

FIGURE- 4.2(a) 20 element mesh for a footing over a layered soil profile with H/B = 0.25

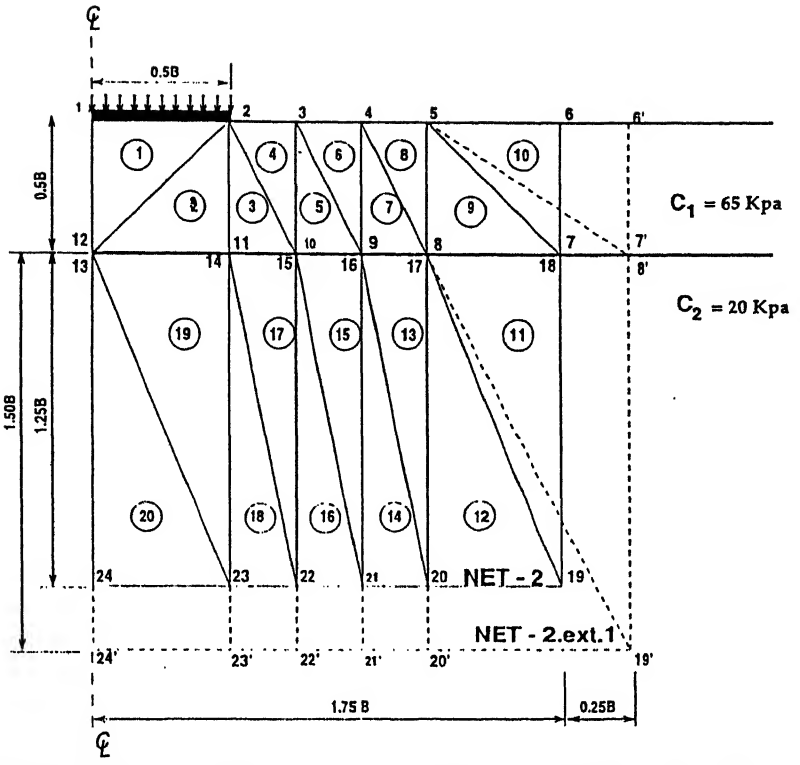

FIGURE- 4.2 (b) 20 element mesh for footing on layered soil profile with H/B = 0.5

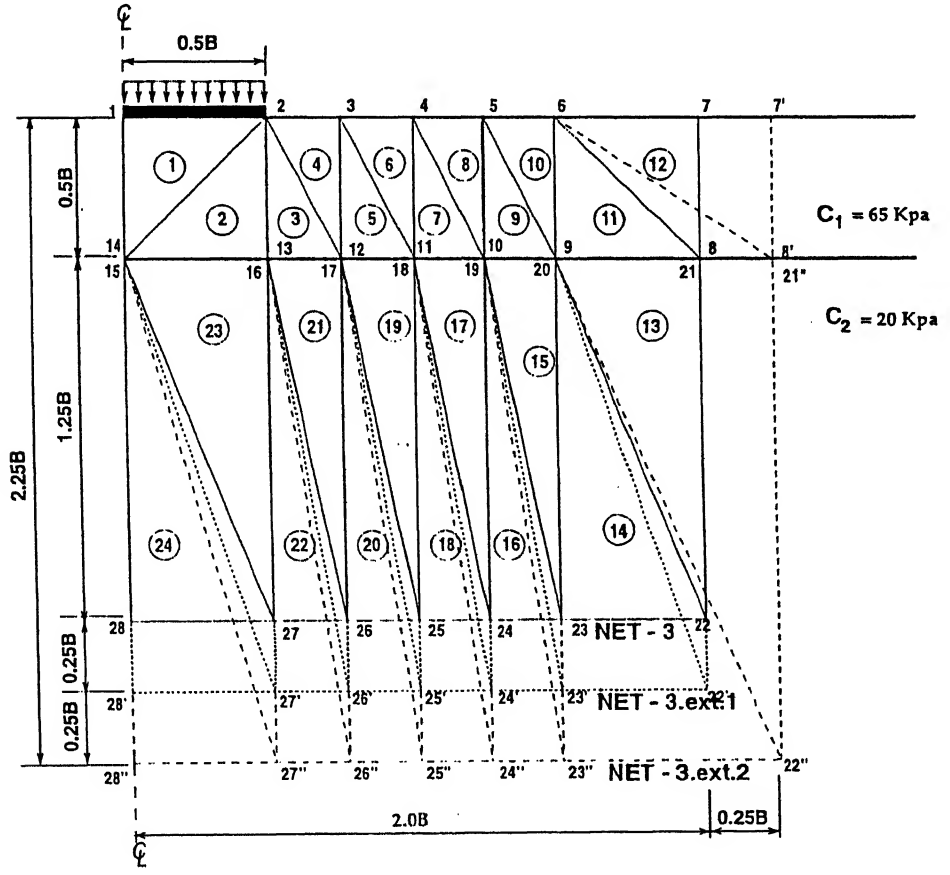

FIGURE- 4.2 (c) 24 element mesh for footing on layered soil profile with H/B = 0.5

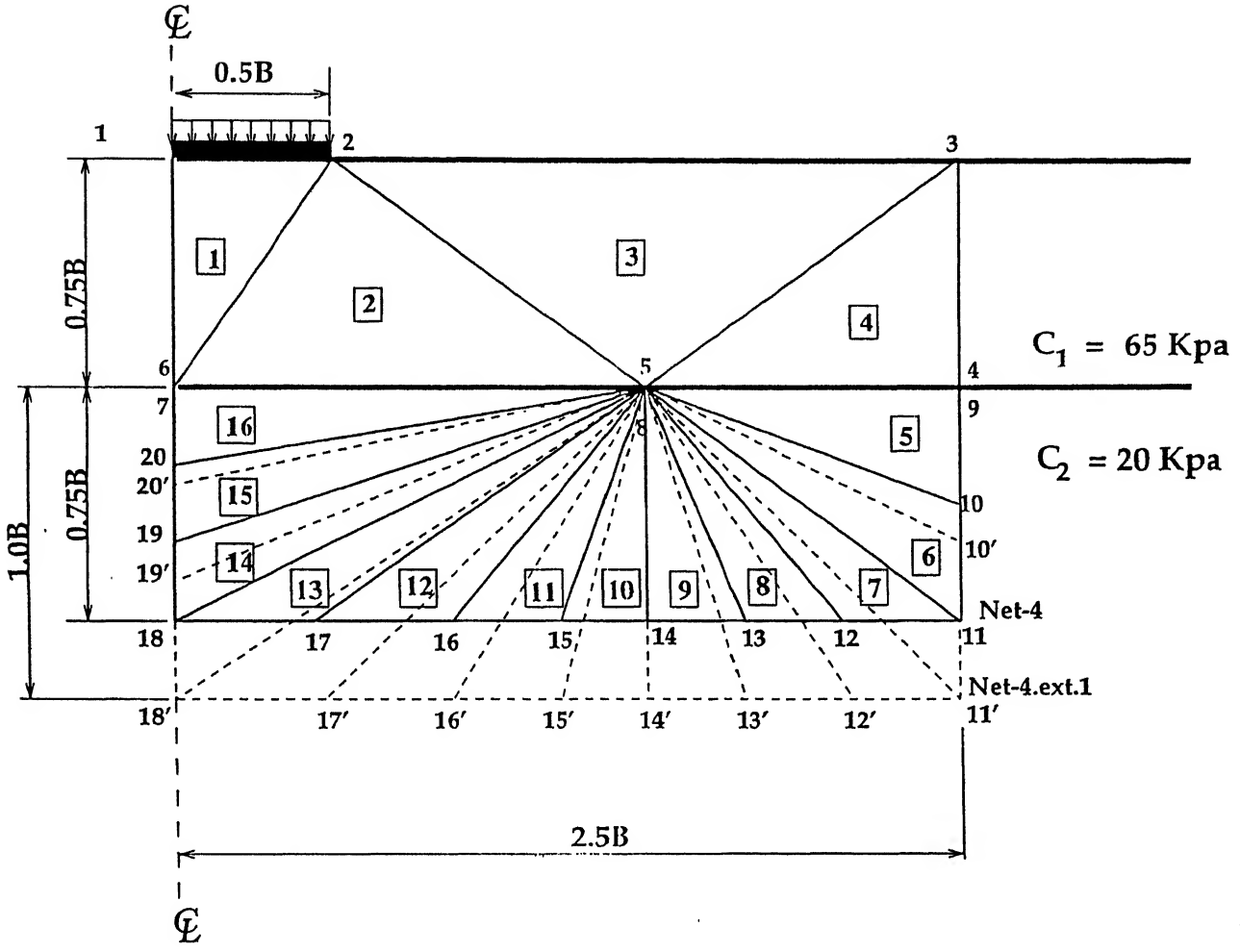

FIGURE-4.2(d) 16 element mesh for footing on layered soil with H/B = 0.75

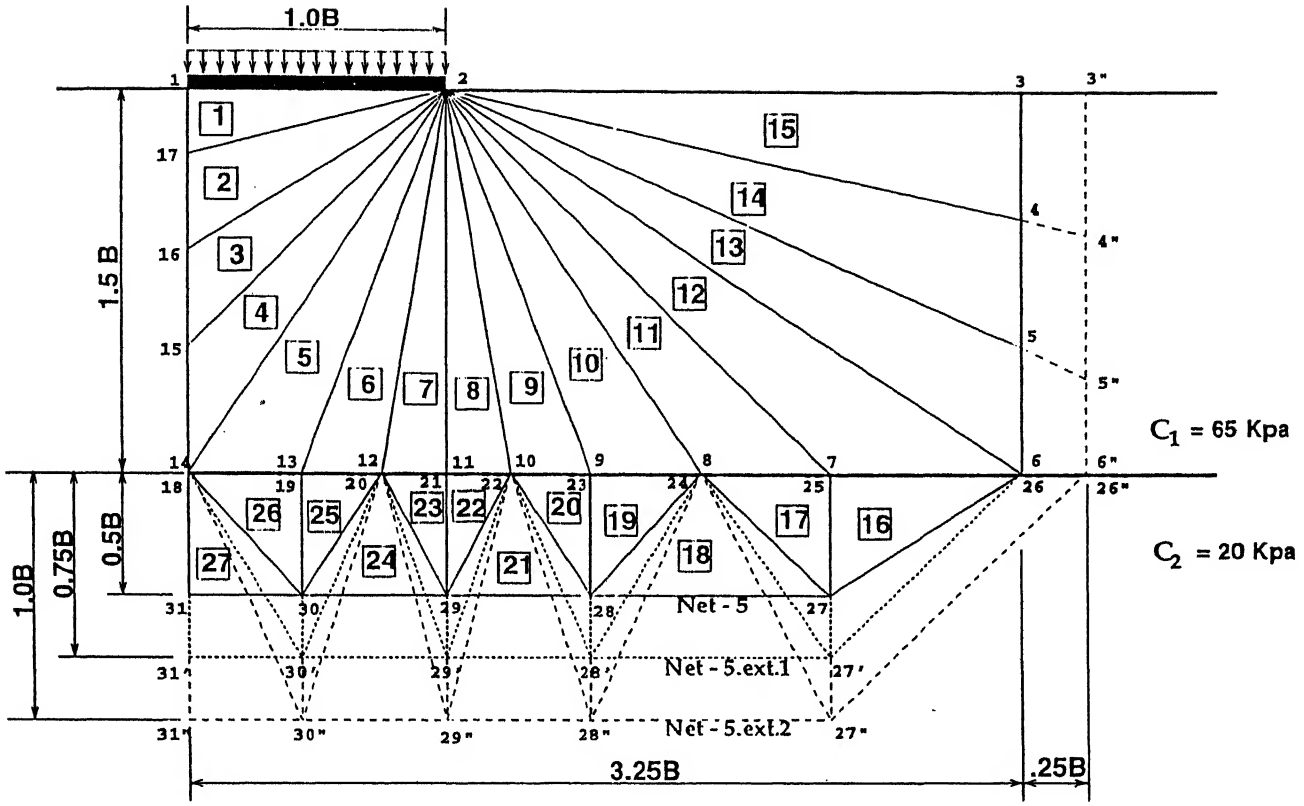

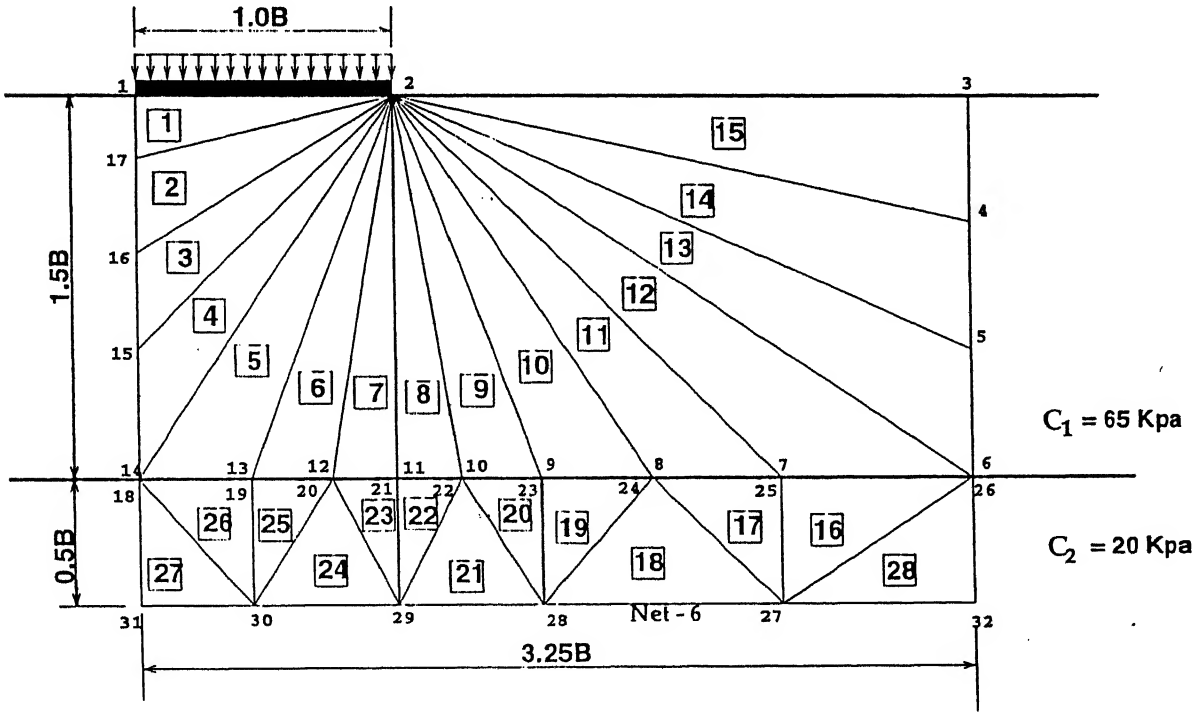

FIGURE-4.2(e) 27 & 28 element meshes for footing on layered soil profile with H / B = 1.5

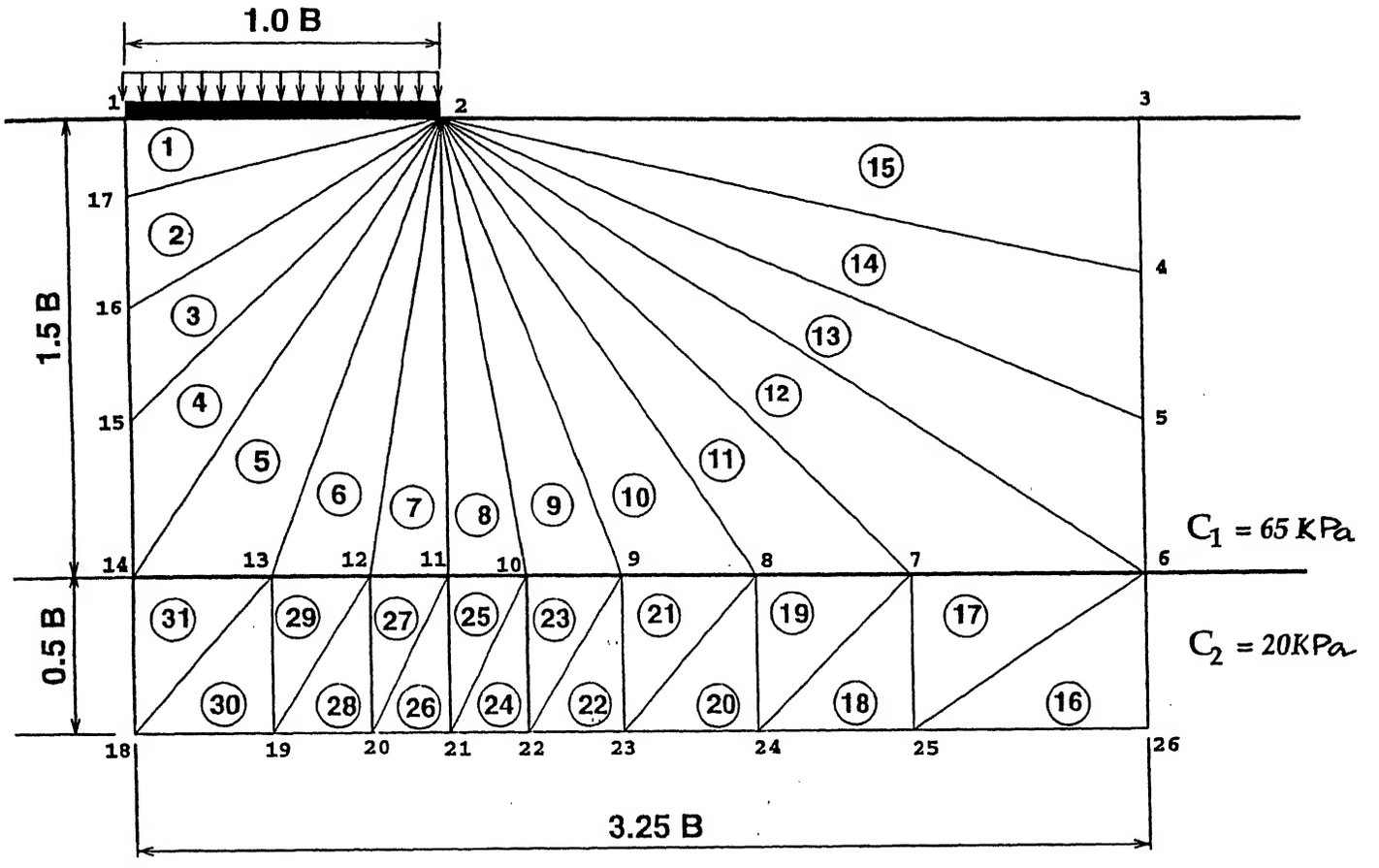

FOR H/B = 1.5

FIGURE - 4.3. 31 element mesh for layered soil profile

(for normal and shear stress continuity case)

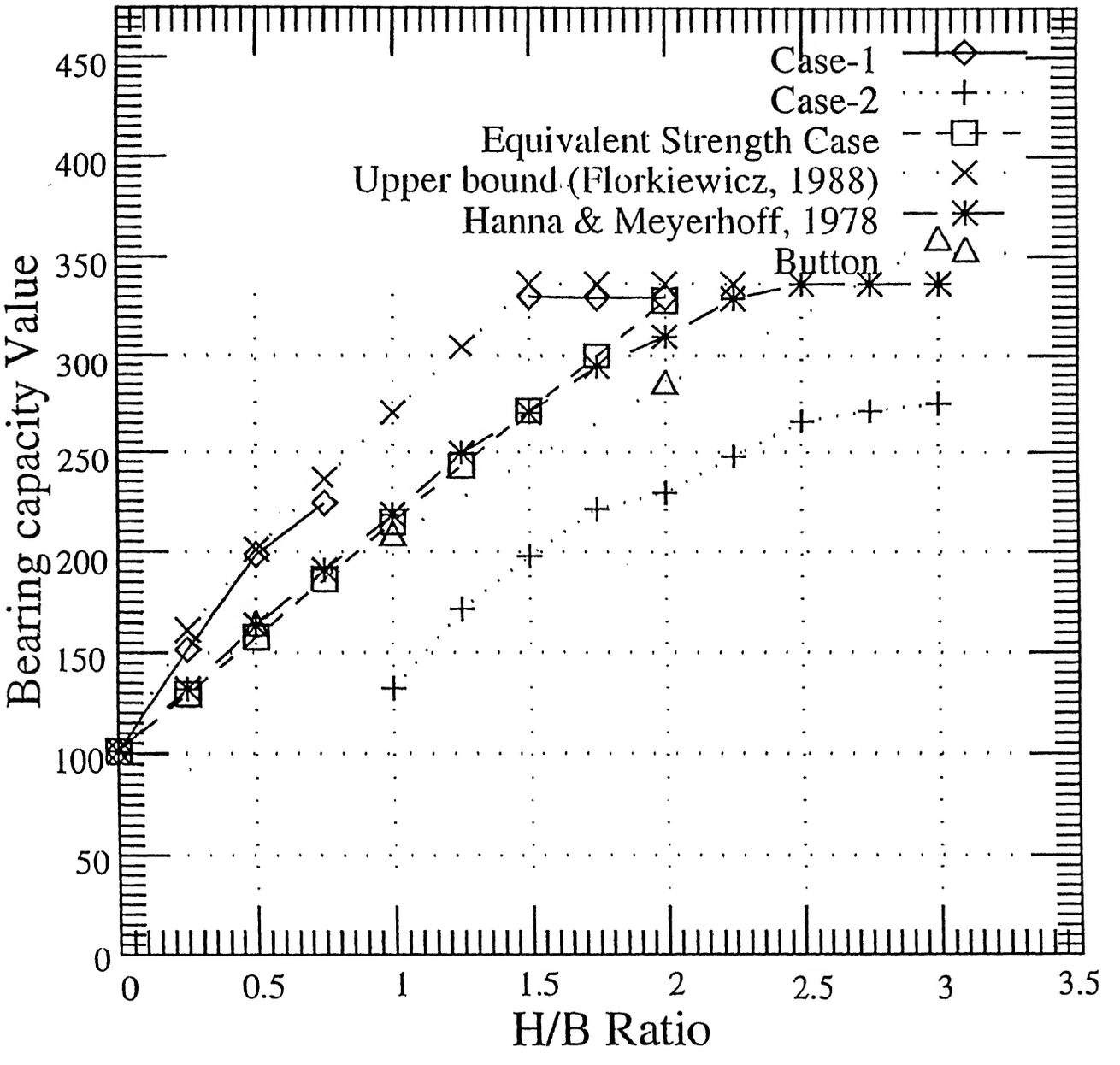

BEARING CAPACITY VALUES Vs H/B RATIO

FIGURE 4.4 Comparision of bearing capacity of footings on two layered soil deposit with other solutions.

Chapter 5

Lower bound bearing capacity of surface strip footings on vertically stratified soil profile.

5.1 Introduction.

It has been observed that vertical stratification in natural soil deposit is not as common as horizontal stratification precisely because of the mechanism involved in the process of formation of the natural deposits. Formation of stratification is the cumulative effect of weathering, transportation and subsequent deposition of materials over a fairly long period of time. Sometimes due to geological movements, a horizontal stratification, may get transformed to a vertical stratification. But still the occurrence of such a soil profile is quite rare.

In comparison to natural occurrence chances of man-made vertical stratification is more in present days of modern engineering practice. Construction of earthen berms for stabilizing existing natural soil profile or built up sections is a common practice. This type of construction invariably results in vertical stratification. Sometimes these berms may have to support certain light temporary, or semi-permanent structure and so it becomes imperative to study the bearing capacity of such soil profile. A study was therefore carried out on the various aspects of such cases. As

a berm or any other such type of earthen structure involves the presence of sloping sides any study for the evaluation of the effect of vertical stratification on the bearing capacity of soil should be done in conjunction with the effect on the slope also.

Chuang (1993) had solved two problems involving vertical stratification for cohesive soil. He had used the failure mechanisms, proposed by Drucker (1953) for the section of two slopes of inhomogeneous, weightless, purely cohesive material, as shown in Fig 5.1(a) and Fig 5.1(b).

Fig 5.1 (a), shows a slope where in the loaded section extends from the topmost corner of the slope to the layer interface. The failure mechanism proposed by Drucker (1953) is valid only for C1 = C2 (homogeneous), $C1 < C2$ or C1/C2 ratio not very large (i.e. inner layer not very weak in comparison to the outer layer). It is because the mechanism assumes that the failure due to the loading does not extend beyond the layer interface. Chuang (1993), chose the shear strength ratio (C1/C2) to be equal to 2.0 and found out that the upper bound solution (3.0487 kPa) was within 0.049% of Drucker's (1953) upper bound solution (3.0472 kPa) for the case.

For the other problem, Fig 5.1(b), it can be seen that the loaded section starts at a distance sufficiently away from the topmost corner of the slope. The left vertical layer,upon which the loading is placed is very stiff in comparison to the other layer, the undrained shear strength ratio (C_1/C_2) of these two layers being equal to 10. For such a case failure could probably occur only the way it has been shown. For this case Chuang (1993) obtained an upper bound bearing capacity (23.5760 kPa) very close to Drucker's (1953) upper bound solution (23.5708 kPa).

These two problems have been chosen as benchmark problems to develop the generalized mesh pattern. The findings are reported under separate headings as follows :

5.2 The Problem .1

Fig 5.2 shows a smooth strip footing of width B lying on the top of a slope of 60^0 inclination over a soil stratum having an undrained shear strength parameter

$C_1 = 1.0$ kPa and adjacent to another soil stratum having undrained shear strength parameter $C_2 = 2.0$ kPa.The loading extends from the left corner of the top of the slope to the layer interface. The objective is to determine the lower bound bearing capacity of this footing and also to find a generalized mesh pattern.

5.2.1 The objective function

The objective functions are :

- -$(\sigma_{1,7} + \sigma_{7,1})$ for Net-1.a.
- -$(\sigma_{1,9} + \sigma_{9,1})$ for Net-1.b, Net-1.b.ext.1 and Net-1.b.ext.2.
- -$(\sigma_{1,10} + \sigma_{10,1})$ for Net-1.c,Net-2, Net-2.ext.1 and Net-2.ext.2.
- -$(\sigma_{1,12} + \sigma_{12,1})$ for Net-3.a and Net-3.b.

Bearing capacity q_f is equal to half of the absolute value of the objective function.

5.2.2 The boundary condition

The boundary conditions for the meshes shown in Fig. 5.2, Fig 5.3 and Fig5.4 are :

For Net-1.a (refer Fig 5.2(a))

$\sigma_{1,2} = \sigma_{2,1} = 0.0$ (*boundary condition*)

$\tau_{1,2} = \tau_{2,1} = 0.0$ (*boundary conditon*)

$\tau_{1,7} = \tau_{7,1} = 0.0$ (*smooth footing*)

For Net-1.b, Net-1.b.ext.1 and Net-1.b.ext.2 (refer Fig 5.2(b))

$\sigma_{1,2} = \sigma_{2,1} = 0.0$ (*boundary condition*)

$\tau_{1,2} = \tau_{2,1} = 0.0$ (*boundary conditon*)

$\tau_{1,9} = \tau_{9,1} = 0.0$ (*smooth footing*)

For Net-1.c (refer Fig 5.2(c))

$$\sigma_{1,2} = \sigma_{2,1} = 0.0 \qquad (boundary \quad condition)$$

$$\tau_{1,2} = \tau_{2,1} = 0.0 \qquad (boundary \quad conditon)$$

$$\tau_{1,10} = \tau_{10,1} = 0.0 \qquad (smooth \quad footing)$$

For Net-2, Net.2.ext.1 (refer Fig 5.3(a)) and Net.2.ext.2 (refer Fig 5.3(b))

$$\sigma_{1,2} = \sigma_{2,1} = 0.0 \qquad (boundary \quad condition)$$

$$\tau_{1,2} = \tau_{2,1} = 0.0 \qquad (boundary \quad conditon)$$

$$\tau_{1,10} = \tau_{10,1} = 0.0 \qquad (smooth \quad footing)$$

For Net-3.a (refer Fig 5.4(a)) and Net-3.b (refer Fig 5.4(b))

$$\sigma_{1,2} = \sigma_{2,1} = 0.0 \qquad (boundary \quad condition)$$

$$\tau_{1,2} = \tau_{2,1} = 0.0 \qquad (boundary \quad conditon)$$

$$\tau_{1,12} = \tau_{12,1} = 0.0 \qquad (smooth \quad footing)$$

5.2.3 Results and Discussions

Initially in finding the lower bound bearing capacity the failure mechanism suggested by Drucker (1953), Fig 5.1(a), was used to generate a mesh pattern (Net-1.a, Fig.5.2(a)). The mesh was studied by varying number of elements from 5 to 7 and then finally to 12. The obtained values corresponding to meshes with 5, 7 and 12 elements are respectively 2.88287 kPa, 2.90122 kPa and 2.90762 kPa which differ by 5.44%, 4.84% and 4.64% respectively on the safer side from the upper bound predicted by Drucker (1953) and Chuang (1993) .The bearing capacity values are very close to each other, the maximum percentage difference between the values being 0.851%. Examination of these values shows that with the increase of the number of elements the bearing capacity value tends to converge to a value of about 2.9 kPa.

Upon extending the Net-1.b with 7 elements (Fig 5.2(b)), the bearing capacity results further improved and with the Net-1.b.ext.1 and Net-1.b.ext.2 the difference from Chuang's upper bound was found to be 2.851% and 0.847%. So for a

better lower bound solution a deeper net is needed. An extra element was then added to Net-1.b.ext.2 to get the Net-1.c (Fig 5.2(c)) to see its effect on the solution. For this case the obtained solution (2.807 kPa) varied only by 7.92% from the Chuang's (1993) upper bound solution (3.0472 kPa).

To find a generalized mesh pattern a mesh pattern with 8 elements as shown in Fig 5.3(a), Net-2, was taken up. The obtained bearing capacity was 2.9777 kPa, which is only 2.32% less than the corresponding upper bound. The Net-2 can be said to be a mesh pattern that does not follow any specific failure mechanism. On extending the Net-2 to Net-2.ext.1 and Net-2.ext.2 (Fig 5.3(b)), the obtained bearing capacity values were 3.00 kPa and 3.00106 kPa which were much better and only 1.59% and 1.51% less than Chuang's upper bound solution. In case of the second extended mesh, (Net-2.ext.2), the solution obtained is the best and further extensions did not yield any improved solution . So it can be concluded that the depth of net exceeding two times the footing width is not necessary for a good solution. However, as far as extensibility of the stress field is concerned the values obtained by the three meshes of Fig 5.3(a) and 5.3(b) varied from each other only by a maximum of 0.94%. It is negligible and the stress field is extensible indicating the obtained bearing capacity values to be the true lower bounds.

From the Fig 5.3(a), Net-2, it can be observed that the element no.8 is bigger in comparison to all the other elements. So the element no.8 was subdivided into three elements (Fig 5.4(a) and Fig 5.4(b)) as shown in Net-3.a and Net-3.b and its effect was studied. When all the elements 10, 9, 8 and 7 were taken to be of equal size (Fig 5.4(a)) a bearing capacity value 2.98050 kPa, 2.37% less than the obtained upper bound . But when the element 10, 9, 8 and 7 were taken as shown in Fig 5.3(b), the result obtained was 2.9896 kPa which is 1.94% less than the upper bound. So it can be safely assumed that the size of element no.10 is not of paramount importance.

The fact that the lower bound value predicted for this case and the upper bound value, as reported by Drucker (1953) and Chuang (1993) are so close to each other, indicates that the critical load lies within the narrow range of 3.0059 kPa and 3.0487 kPa.

It can be concluded that Net-2.ext.2, which is a generalized mesh pattern,

can be used for finding the lower bound bearing capacity values for strip footing on slopes involving vertical stratification. . . . The stress field and the stress-strength ratio obtained for the Net-2.ext.2 is presented in Table 5.1. The stress field is excellent because the stress-strength ratio at different nodal points for all the elements are very close to unity thus signifying the limiting equilibrium state. The depth of the net need not exceed two times the footing width to give values which are in very good agreement with upper bound solution. A mesh with 8 elements was found to be sufficient. All the N_c values obtained by the various meshes are presented in Table 5.2.

As Net-2.ext.2 had produced the best lower bound solution for this case the same mesh pattern was used to find the lower bound bearing capacity for footing on slopes with the slope angles varying from 0^0 to 90^0. The results are presented in Table 5.3 and graphically in Fig 5.5. N_c and the slope angle bears a linear relationship.

The lower bound bearing capacity factors N_c for various slopes can be represented by the following equation.

$$N_c = 5.03317 - 0.03417(\beta)$$

where β is the slope angle in degrees.

$$q_f = N_c C_1$$

The values obtained could not be compared with any other reported solution except the one reported by Drucker (1953) and Chuang (1993) for 60^0 slope due to lack of data.

5.3 The Problem .2

Fig 5.6 shows a smooth strip footing of width B lying at a distance sufficiently away from the slope. It rests over a very stiff soil stratum having an undrained shear strength parameter C_1 = 10.0 kPa and and extends up to the layer interface. The adjacent weaker soil stratum has an undrained shear strength C_2 = 1.00 kPa. The objective is to determine the lower bound bearing capacity of this footing using a generalized mesh pattern.

This same problem was solved by Chuang (1993) and the results were compared with Drucker's (1953) upper bound solution for validation. The collapse mechanism chosen was as suggested by Drucker (1953)

5.3.1 The objective function

The objective functions are:

- -($\sigma_{1,7} + \sigma_{7,1}$) for Net-4.a
- -($\sigma_{1,10} + \sigma_{10,1}$) for Net-4.b and Net-4.b.ext.1
- -($\sigma_{1,2} + \sigma_{2,1}$) for Net-5, Net-5.ext.1, Net-6, Net-6.ext.1

The bearing capacity q_f is equal to half of the absolute value of the objective function.

5.3.2 The Boundary Conditions

The boundary conditions for the meshes shown in Fig. 5.6, Fig.5.7 and Fig.5.8 are:

For Net-4.a (refer Fig 5.6(a))

$\sigma_{6,7} = \sigma_{7,6} = 0.0$ (*boundary condition*)

$\tau_{6,7} = \tau_{7,6} = 0.0$ (*boundary conditon*)

$\tau_{1,7} = \tau_{7,1} = 0.0$ (*smooth footing*)

For Net-4.b and Net-4.b.ext.1 (refer Fig 5.6(b))

$\sigma_{9,10} = \sigma_{10,9} = 0.0$ (*boundary condition*)

$\tau_{9,10} = \tau_{10,9} = 0.0$ (*boundary conditon*)

$\tau_{1,10} = \tau_{10,1} = 0.0$ (*smooth footing*)

For Net-5 and Net-5.ext.1 (refer Fig 5.7)

$\sigma_{2,3} = \sigma_{3,2} = 0.0$ (*boundary condition*)

$\tau_{2,3} = \tau_{3,2} = 0.0$ (*boundary conditon*)

$\tau_{1,2} = \tau_{2,1} = 0.0$ (*smooth footing*)

For Net-6 and Net-6.ext.1 (refer Fig 5.8)

$$\sigma_{2,3} = \sigma_{3,2} = 0.0 \qquad (boundary \quad condition)$$

$$\tau_{2,3} = \tau_{3,2} = 0.0 \qquad (boundary \quad conditon)$$

$$\tau_{1,2} = \tau_{2,1} = 0.0 \qquad (smooth \quad footing)$$

5.3.3 Results and discussions.

Similar to the previous case, the Net-4.a, Fig 5.6.(a), considered for this case was based on the Drucker's mechanism (Fig 5.1(b)) . Results were obtained by varying the number of elements. The results obtained for 5, 8 and 14 element mesh patterns are 20.4969 kPa, 20.0662 kPa and 20.1060 kPa which are 13.06% 14.89% and 14.71% lower than the upper bound solution (23.5760 kPa) reported by Chuang (1993). So increase in the number of elements did not result in any improvement in the lower bound solution. The mesh with 8 elements , (Fig 5.6.(b)), was extended as shown and the obtained result (20.0931 kPa) was found to be lower than the upper bound by 14.35% only and different from the value obtained by Net-4.b by only 0.15%. This means that the considered stress-field is extensible and the obtained solution is a true lower bound solution.

To improve upon the results, a second mesh (Net-5, Fig 5.7) with 15 elements based on Prandtl's surface (for homogeneous soil profile) was tried out. Interestingly the obtained lower bound bearing capacity was 23.100 kPa, which is only 1.98% less than that of the upper bound solution reported by Chuang. Upon extension of the mesh as shown in Fig 5.7, a value of 23.159 kPa was obtained which was only 1.77% less from the upper bound and different from the result obtained by the original Net-5, by only 0.212%,thus demonstrating the extensibility of the stress-field. The fact that the difference between the lower bound and the upper bound is of the order of 1.7% shows that the true value of the critical load lies within a narrow range of 23.159 kPa and 23.576 kPa.

Further in the endevour to obtain a generalized mesh pattern devoid of any influence of failure mechanism a third mesh, Net-6, as shown in Fig 5.8 was chosen.

This was arrived at by extending the Net-5, with 15 elements over a rectangular domain. The value of bearing capacity found by the Net-6 was 23.237 kPa which differed only by 1.44% from Chuang's upper bound solution. The net was extended further as shown in Fig 5.8, by dotted lines. The values obtained for the extension-1 and extension-2 are 23.3346 kPa and 23.2159 kPa respectively. The two bearing capacity values obtained by the extension of the original mesh pattern (Net-5) differ from it by only 0.418% and 0.09%. So it can be concluded that the stress-field generated by the mesh pattern suggested by Net-6, is extensible and therefore predicts the true lower bound. The complete stress field along with the stress-strength ratio obtained for the Net-6.ext.2, which happens to give the best solution has been presented in Table 5.4. It can be seen from the table that the limiting equilibrium state has been reached as the stress-strength ratio at different nodal points for all the elements are very close to unity.

The fact that the difference between the lower bound and the upper bound is of the order of 1.02% shows that the true value of the critical load lies within a narrow range of 23.3346 kPa and 23.576 kPa.

All the lower bound bearing capacity values for this case ($C_1/C_2 = 10.0$) obtained by the various nets are tabulated in Table 5.5. It can be seen that the maximum and minimum percentage difference from Chuang's (1993) upper bound solution is 14.89% (Net-4.b) and 1.024% (Net-6.ext.1). Also it can be observed that solutions obtained by the generalized mesh pattern (Net-6 and its extension) are very close to the upper bound solution of Chuang, the maximum percentage difference being only 1.44% .

It has been found from these studies that a depth of net (Net-6.ext.1) of 1.75 times the footing width and a horizontal extent of 3.5 times of the footing width give very good lower bound solution. With the Net-6, and taking smooth footing condition, a study has been conducted for various C1/C2 ratio. The values are tabulated in Table 5.6 and also graphically presented in Fig 5.9. These obtained values could not be compared with other solution except for $C_1/C_2 = 10.0$ which has been reported by Drucker (1953) and Chuang (1993), due to lack of data.

From the Fig 5.9 it is very clear that bearing capacity and C_1/C_2 ratio bears

a straight line relation. So lower bound bearing capacity for soil profile with vertical stratification can be represented by the following equation when $C_1/C_2 \geq 1.0$.

$$q_f = 2.01622C_1/C_2 + 0.30565$$

5.4 Conclusions

For the two specific cases of strip footings on vertically stratified deposits, based on the results and discussions as presented the following conclusions can be drawn:

1. True lower bound solutions in very close agreement with upper upper bound solution reported by Drucker (1953) can be obtained by using the extended Lysmer's method. The lower and the upper bound being very close gives an indication of the actual critical load within a very narrow range.

2. Generalized mesh pattern devoid of influence of any possible failure mechanism have been developed for both the cases.

3. For vertically stratified soil, the footing resting on the top of a slope and only on the first layer, the bearing capacity factor N_c bears a linear relationship with slope angle β. The relation being

$$N_c = 5.03317 - 0.03417(\beta)$$

4. For footings lying on a stiff soil adjacent to a weaker vertical layer the bearing capacity and the C_1/C_2 ratio bears a linear relationship as given below.

$$q_f = 2.01622C_1/C_2 + 0.30565$$

Table 5.1

Stress Field and Stress-Strength Ratios at the Nodal Points for Net-2.ext.2

8 element net

Element No.	Nodal Point	σ_x	σ_z	τ_{zx}	Stress Strength ratio
1	1	0.546502E+00	0.144491E+01	0.888621E+00	0.991433E+00
1	2	0.546572E+00	0.144510E+01	0.888735E+00	0.991686E+00
1	3	0.533229E+00	0.140971E+01	0.867004E+00	0.943749E+00
2	1	0.544508E+00	0.143400E+01	0.883956E+00	0.979177E+00
2	3	0.540269E+00	0.144823E+01	0.883472E+00	0.986622E+00
2	4	0.530309E+00	0.138883E+01	0.860356E+00	0.924477E+00
3	1	0.545937E+00	0.145398E+01	0.889300E+00	0.996988E+00
3	4	0.535962E+00	0.146782E+01	0.881486E+00	0.994109E+00
3	5	0.530250E+00	0.139683E+01	0.864625E+00	0.935315E+00
4	1	0.545021E+00	0.138319E+01	0.881248E+00	0.952229E+00
4	5	0.531478E+00	0.149176E+01	0.875422E+00	0.996897E+00
4	6	0.530943E+00	0.137292E+01	0.878596E+00	0.949160E+00
5	1	0.545216E+00	0.150468E+01	0.876388E+00	0.998197E+00
5	6	0.531136E+00	0.149330E+01	0.873781E+00	0.994933E+00
5	7	0.530826E+00	0.150637E+01	0.871509E+00	0.997449E+00
6	1	0.527850E+00	0.104209E+01	0.966014E+00	0.999294E+00
6	7	0.513962E+00	0.105712E+01	0.958550E+00	0.992574E+00
6	8	0.513725E+00	0.109160E+01	0.954087E+00	0.993767E+00
7	1	0.539154E+00	0.113916E+01	0.932890E+00	0.960285E+00
7	8	0.513291E+00	0.108788E+01	0.955356E+00	0.995244E+00
7	9	0.515227E+00	0.105002E+01	0.960138E+00	0.993364E+00
8	1	0.100560E+01	0.300494E+01	0.155523E-06	0.999339E+00
8	9	0.100202E+01	0.299719E+01	0.134486E-01	0.995355E+00
8	10	0.998875E+00	0.299719E+01	0.268221E-06	0.998314E+00

Table 5.2 N_c VALUES OBTAINED BY DIFFERENT MESH PATTERNS

for a footing on the top of a slope of 60^0 *inclination*

Net Used	Number of elements	Figure number	Net_c value	% diff. from Chuang's Upper Bound
Net-1.a	5	Fig 5.2(a)	2.88287	5.44%
Net-1.b	7	Fig 5.2(b)	2.90122	4.84%
Net-1.b.ext.1	7	Fig 5.2(b)	2.96180	2.85%
Net-1.b.ext.2	7	Fig 5.2(b)	3.02288	0.85%
Net-1.c	12		2.90726	4.64%
Net-1.d	8	Fig 5.2(c)	2.80700	7.92%
Net-2	8	Fig 5.3(a)	2.97770	2.32%
Net-2.ext.1	8	Fig 5.3(a)	3.00001	1.59%
Net-2.ext.2	8	Fig 5.3(b)	3.00106	1.51%
Net-3.a	10	Fig 5.4(a)	2.98050	2.37%
Net-3.b	10	Fig 5.4(b)	2.98960	1.94%

Table 5.3 N_c VALUES FOR FOOTINGS ON THE TOP OF A SLOPE

for various slope angles

SLOPE ANGLES	Lower Bound N_c Values
0.0^0	5.0480
10.0^0	4.6642
20.0^0	4.3355
30.0^0	4.0235
40.0^0	3.6821
45.0^0	3.4750
50.0^0	3.3205
60.0^0	3.0229
70.0^0	2.6659
80.0^0	2.2506
90.0^0	1.9617

Table 5.4

Stress Field and Stress-Strength Ratios at the Nodal Points for Net-5.ext.1

15 element net

Element No.	Nodal Point	σ_x	σ_z	τ_{zx}	Stress Strength ratio
1	2	0.355188E+01	0.232337E+02	0.190735E-05	0.968432E+00
1	1	0.343703E+01	0.234356E+02	0.190735E-05	0.999858E+00
1	17	0.343887E+01	0.234356E+02	0.574245E-01	0.999707E+00
2	2	0.321546E+01	0.231496E+02	0.168211E+00	0.993704E+00
2	17	0.343969E+01	0.234358E+02	0.578289E-01	0.999645E+00
2	16	0.321548E+01	0.232107E+02	0.166386E+00	0.999796E+00
3	2	0.257693E+01	0.225110E+02	0.806761E+00	0.999929E+00
3	16	0.341950E+01	0.234147E+02	0.376377E-01	0.999534E+00
3	15	0.190339E+01	0.212660E+02	0.179444E+01	0.969474E+00
4	2	0.243300E+01	0.222389E+02	0.100464E+01	0.990780E+00
4	15	0.245423E+01	0.223074E+02	0.103703E+01	0.996126E+00
4	14	0.248496E+01	0.223667E+02	0.100275E+01	0.998266E+00
5	2	0.246488E+01	0.223365E+02	0.948866E+00	0.996208E+00
5	14	0.247961E+01	0.223503E+02	0.101212E+01	0.997356E+00
5	13	0.246338E+01	0.223369E+02	0.101680E+01	0.997735E+00
6	2	0.247080E+01	0.223830E+02	0.932287E+00	0.999927E+00
6	13	0.246372E+01	0.223396E+02	0.101584E+01	0.997950E+00
6	12	0.244128E+01	0.223079E+02	0.103523E+01	0.997422E+00
7	2	0.246027E+01	0.220246E+02	0.993723E+00	0.966780E+00
7	12	0.244132E+01	0.223096E+02	0.103495E+01	0.997577E+00
7	11	0.244301E+01	0.223224E+02	0.983898E+00	0.997654E+00
8	2	0.246027E+01	0.225310E+01	0.993725E+00	0.998219E+00
8	11	0.244301E+01	0.242553E+01	0.983896E+00	0.968128E+00
8	10	0.244469E+01	0.217309E+01	0.954338E+00	0.929204E+00
9	2	0.245817E+01	0.218179E+01	0.981501E+00	0.982440E+00
9	10	0.244034E+01	0.202506E+01	0.928964E+00	0.906090E+00
9	9	0.244195E+01	0.153927E+01	0.877033E+00	0.972896E+00

contd. on next page

Table 5.4

Element No.	Nodal Point No.	σ_x	σ_z	τ_{zx}	Stress Strength ratio
10	2	0.221029E+01	0.385010E+00	0.314118E+00	0.931578E+00
10	9	0.233171E+01	0.740172E+00	0.580223E+00	0.969903E+00
10	8	0.216111E+01	0.369097E+00	0.335846E+00	0.915616E+00
11	2	0.209888E+01	0.137886E+00	0.148196E+00	0.983341E+00
11	8	0.207745E+01	0.183522E+00	0.211248E+00	0.941364E+00
11	7	0.202099E+01	0.126570E+00	0.158014E+00	0.922174E+00
12	2	0.203545E+01	0.744573E-01	0.847658E-01	0.968559E+00
12	7	0.198113E+01	0.867138E-01	0.118158E+00	0.911166E+00
12	6	0.204010E+01	0.168510E+00	0.193827E+00	0.913284E+00
13	2	0.179579E+01	-0.320602E-01	0.750088E-01	0.840887E+00
13	6	0.138177E+01	-0.124081E+00	0.245062E+00	0.626954E+00
13	5	0.184928E+01	-0.182561E-01	0.280200E-01	0.872712E+00
14	2	0.195866E+01	-0.801302E-03	0.365812E-02	0.959881E+00
14	5	0.193733E+01	-0.135729E-02	0.105529E-01	0.939739E+00
14	4	0.193657E+01	-0.436485E-03	0.554897E-02	0.938031E+00
15	2	0.197536E+01	0.000000E+00	0.523565E-07	0.975509E+00
15	4	0.194567E+01	-0.223517E-07	0.754154E-02	0.946462E+00
15	3	0.194093E+01	0.000000E+00	0.149012E-06	0.941801E+00

Table 5.5 LOWER BOUND BEARING CAPACITY VALUES OBTAINED BY DIFFERENT MESH PATTERNS

for a footing lying on the top of a stiff soil adjacent to a weaker soil

Net Used	Number of elements	Figure number	Bearing Capacity kPa	% diff. from Chuang's Upper Bound
Net-4.a	5	Fig 5.6(a)	20.4969	13.06%
Net-4.b	8	Fig 5.6(b)	20.0662	14.89%
Net-4.b.ext.1	8	Fig 5.6(b)	20.0931	14.35%
Net-4.c	14		20.1060	14.71%
Net-5	15	Fig 5.7	20.1100	1.98%
Net-5.ext.1	15	Fig 5.7	23.1590	1.77%
Net-6	15	Fig 5.8	23.2370	1.44%
Net-6.ext.1	15	Fig 5.8	23.3346	1.02%
Net-6.ext.2	15	Fig 5.8	23.2159	1.53%

Table 5.6 LOWER BOUND BEARING CAPACITY VALUES

for various C_1/C_2 ratio

C_1/C_2 ratio	Lower bound Bearing Capacity (in kPa)
1.0	5.048
2.0	7.165
3.0	9.047
4.0	11.130
5.0	13.255
6.0	15.117
7.0	17.121
8.0	19.008
9.0	21.229
10.0	23.334

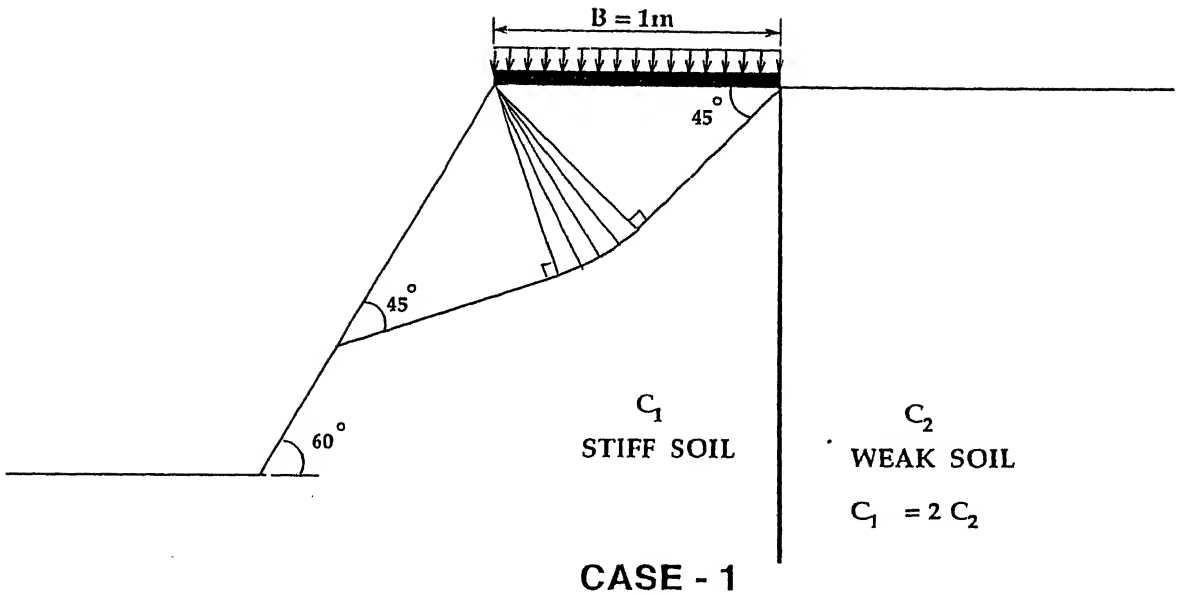

FIGURE-5.1 (a) Details of a surface strip footing placed on the edge of a slope adjacent to a weaker layer

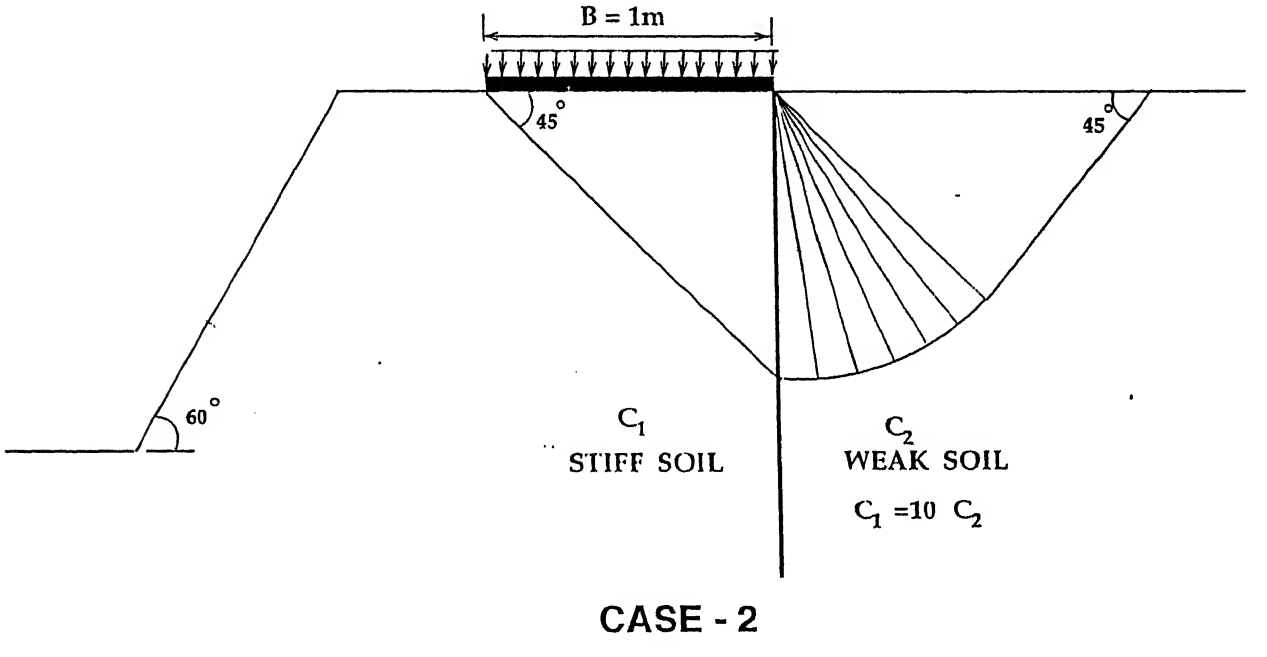

FIGURE-5.1 (b) Details of a surface strip footing placed away from the slope adjacent to a weaker layer

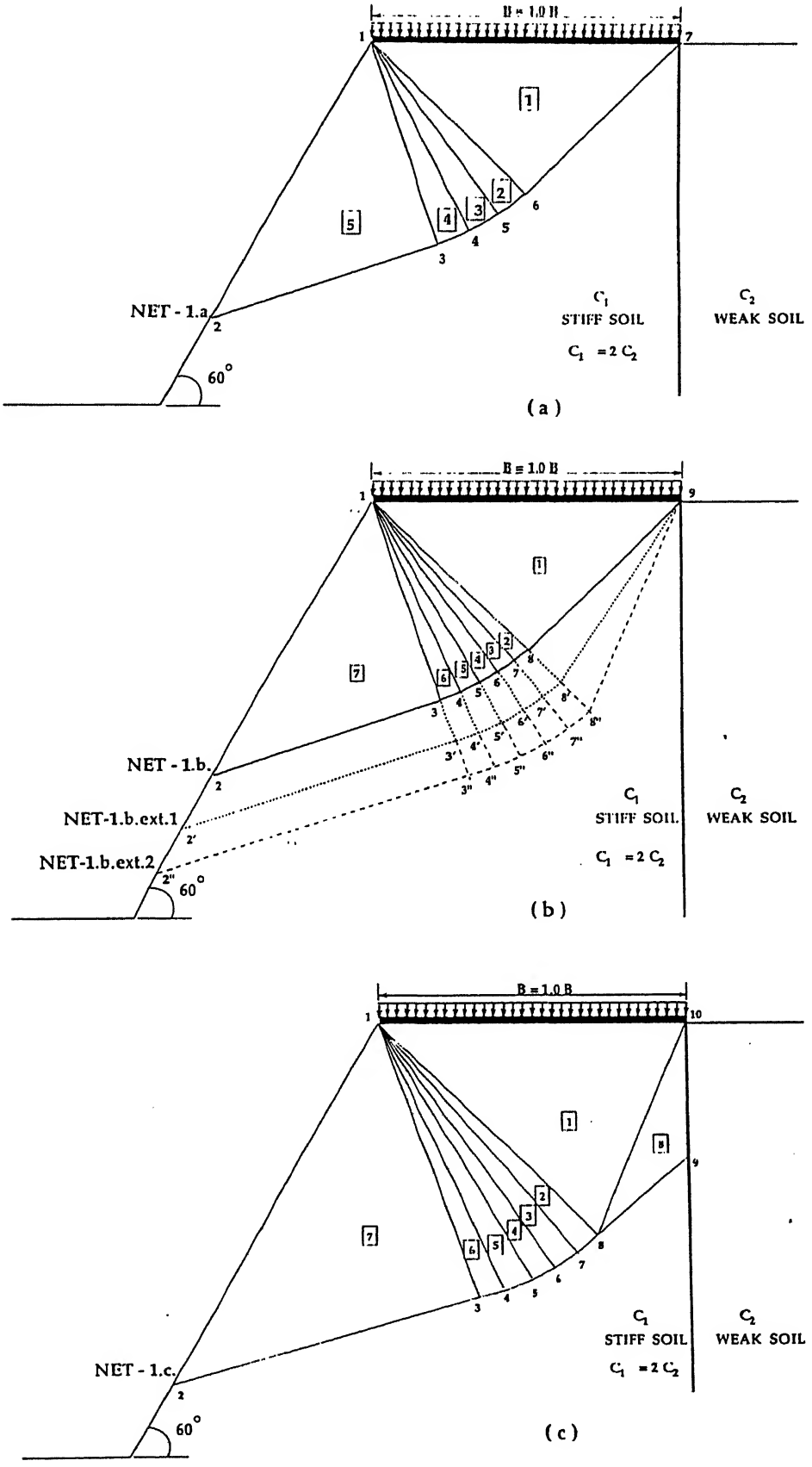

FIGURE 5.2 Mesh Patterns with 5, 7 and 8 elements for Case -1 of Vertically stratified soil profile.

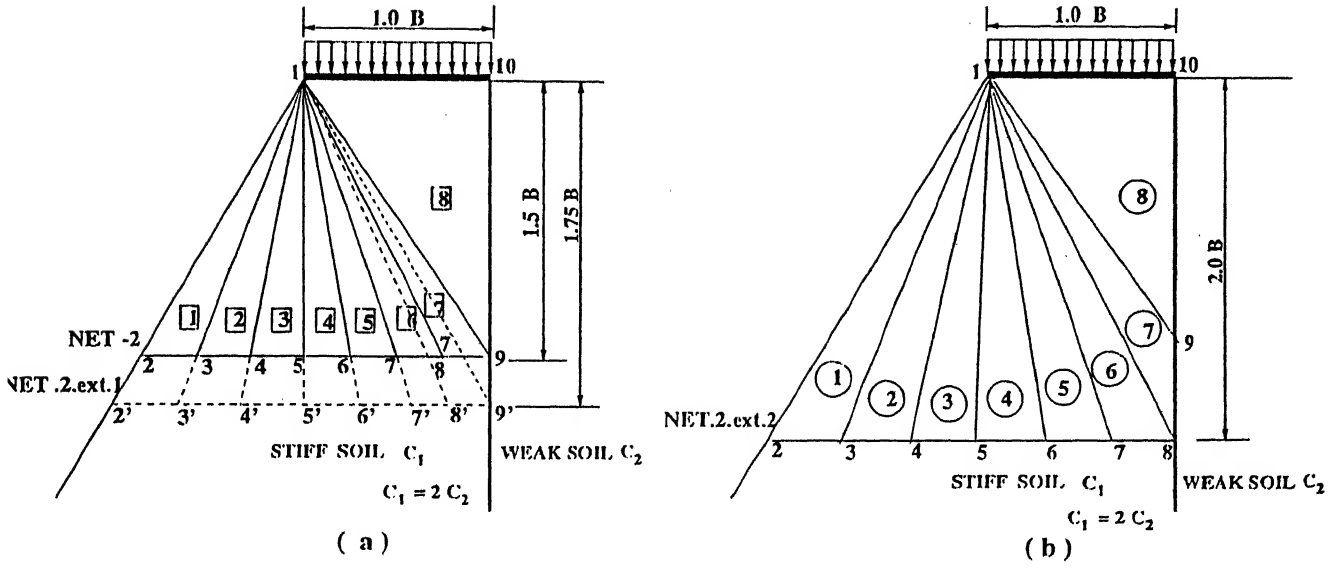

FIGURE - 5.3 Generalized mesh pattern (8 elements) for Case-1 of vertically stratified soil profile

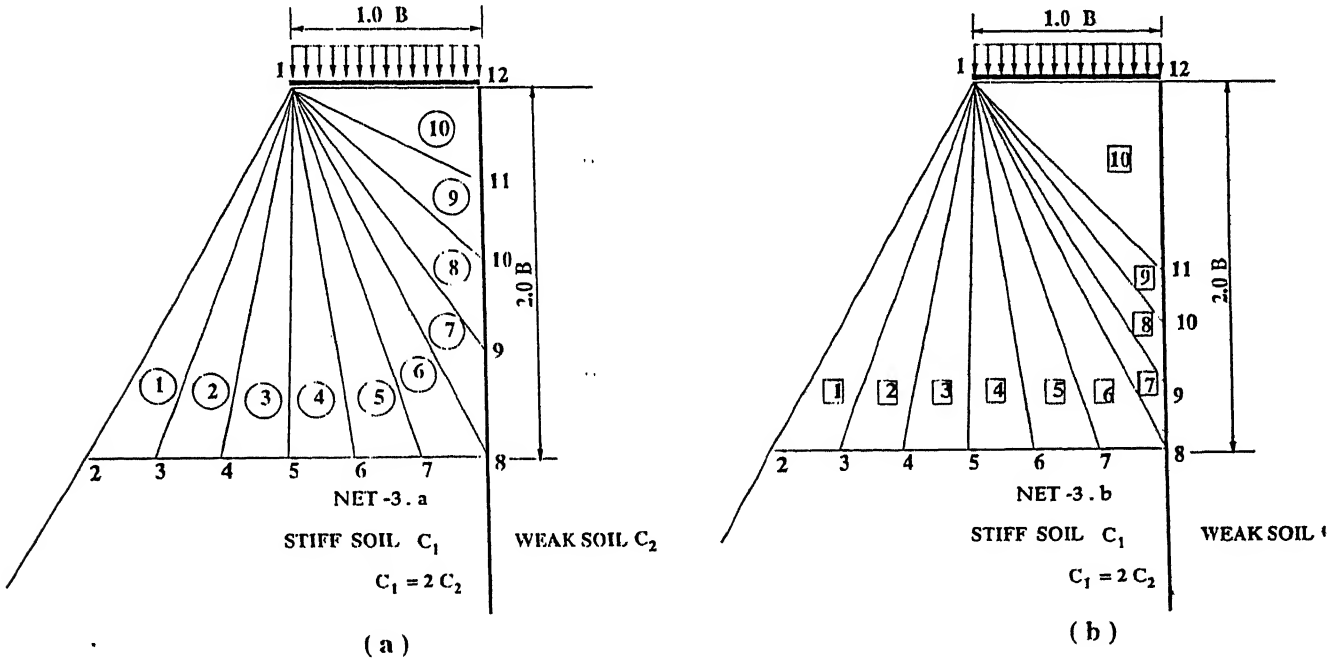

FIGURE - 5.4 Generalized mesh pattern (10 elements) for Case-1 of vertically stratified soil profile

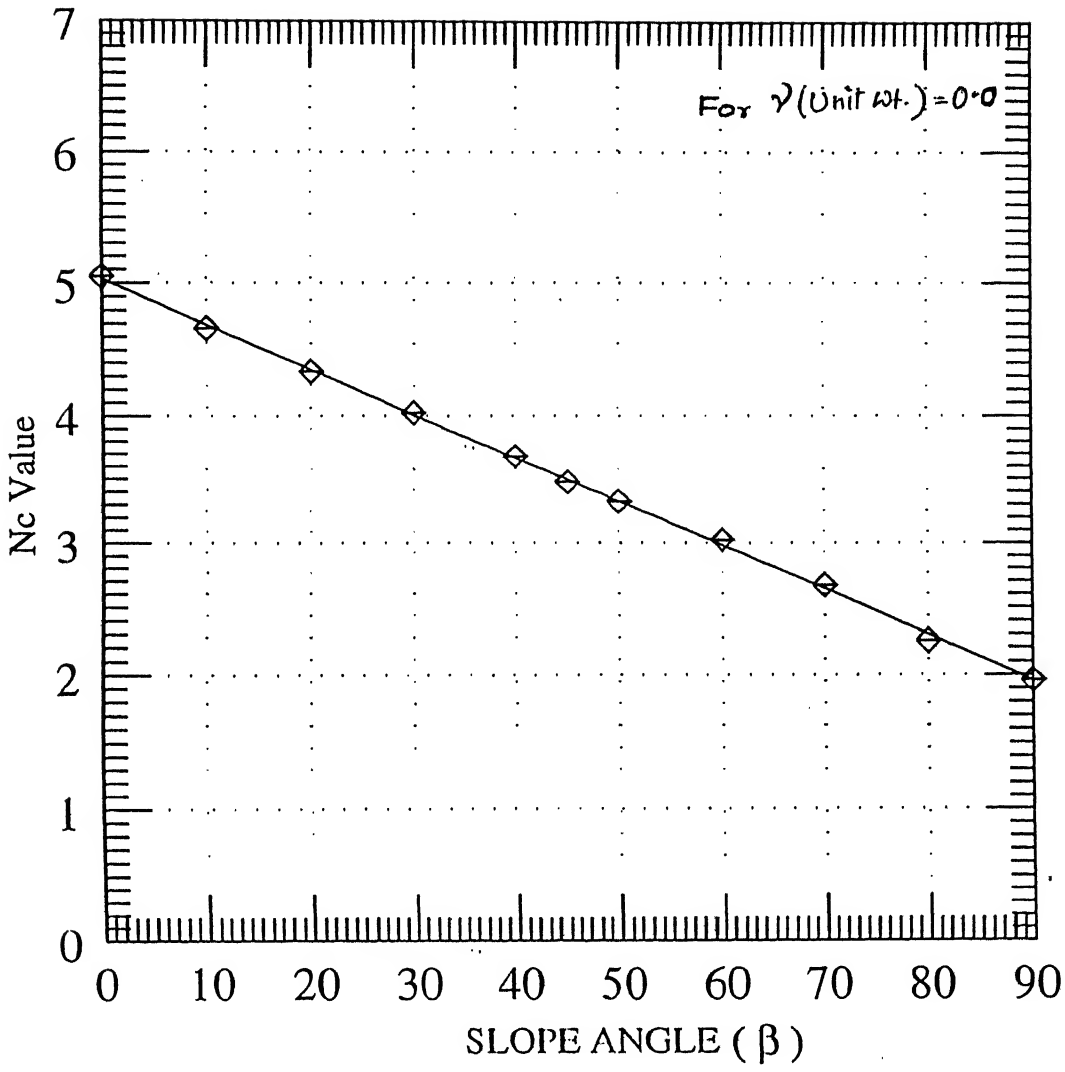

Nc VALUES Vs. SLOPE ANGLE

$$N_c = 5.03317 - 0.03417 (\beta)$$

FIGURE 5.5 variation of N_c value with slope angle(β)

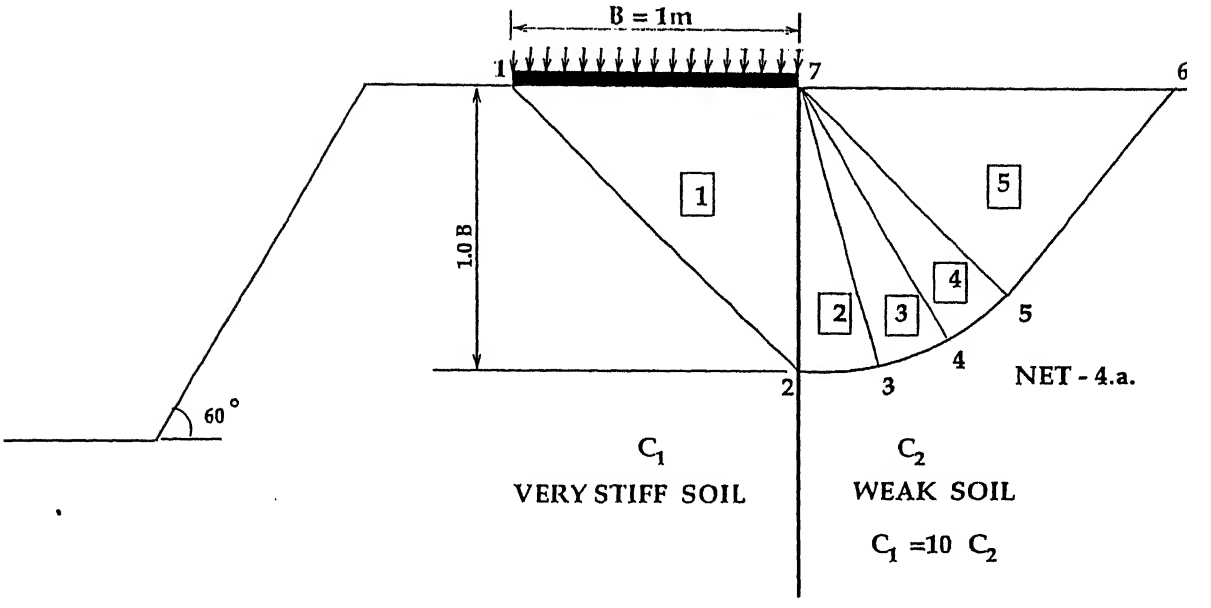

(a)

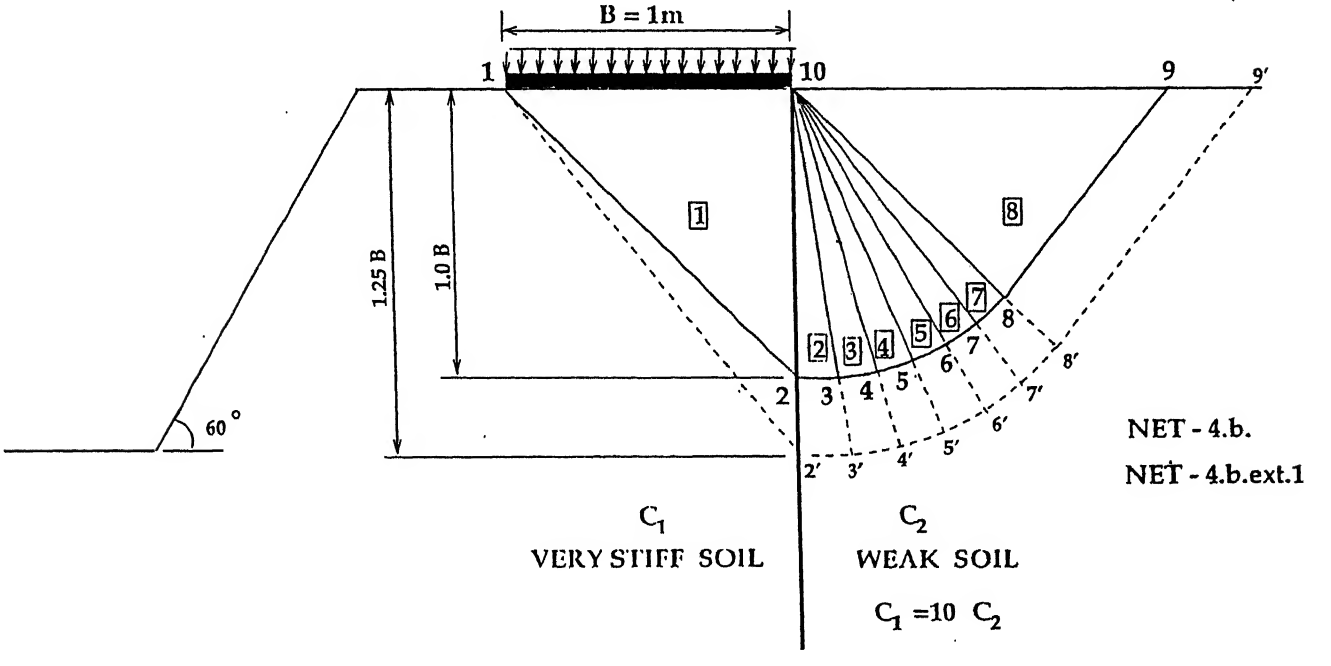

(b)

FIGURE -5.6 Mesh patterns with 5 & 8 elements for Case-2 of vertically stratified soil profile.

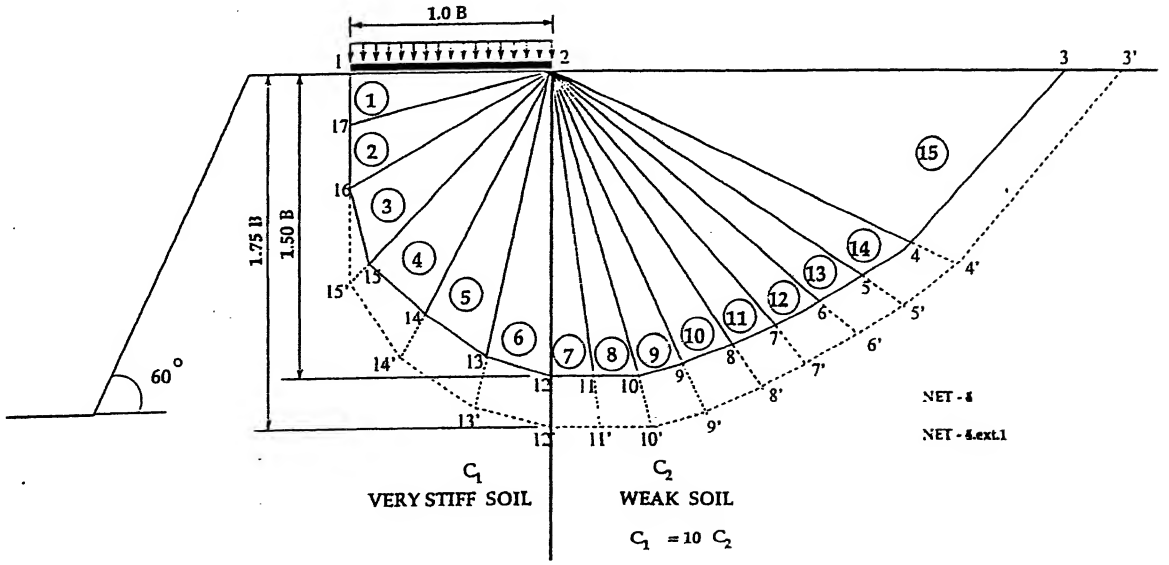

FIGURE 5.7 15 element mesh pattern for Case-2

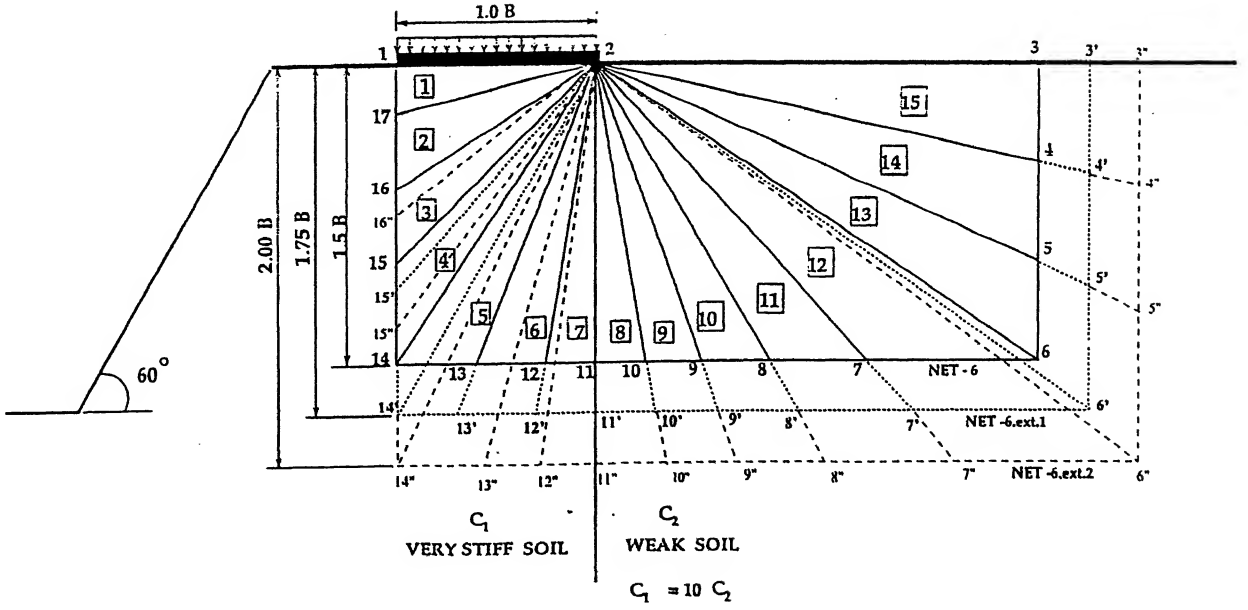

FIGURE 5.8 Generalized mesh pattern for Case-2

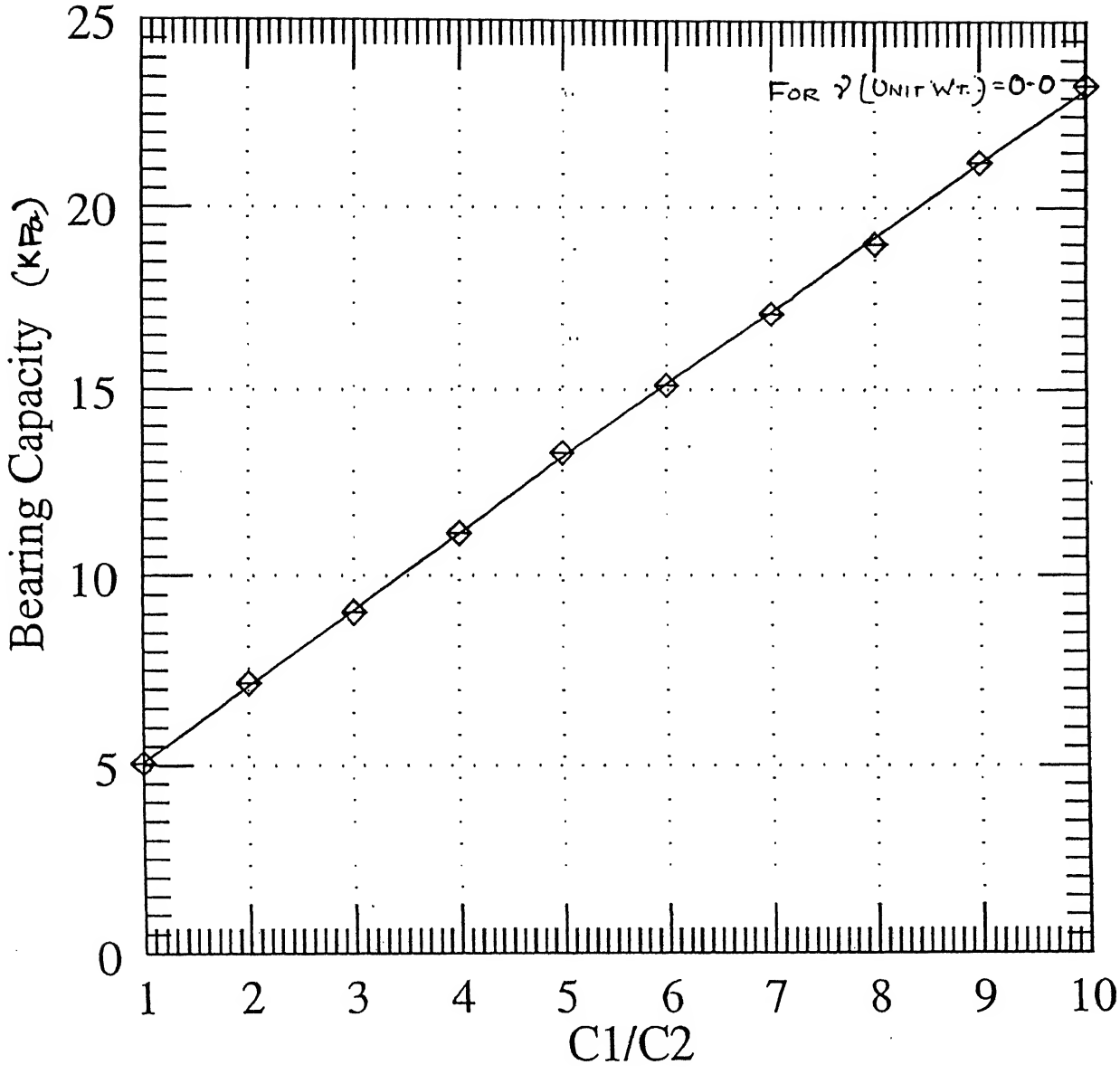

BEARING CAPACITY Vs C1/C2 RATIO for layered soil

BEARING CAPACITY = 2.01622 C_1/C_2 + 0.30565

FIGURE 5.9 Variation of Bearing Capacity with C_1 / C_2 ratio

Chapter 6

Scope of Future Work

The following topics are suggested for future studies.

1. For a two layered (horizontal) soil system trial should be made to develop a mesh pattern for $0.75 < H/B < 1.5$ to obtain the lower bound values considering stress discontinuity at the layer interface. Studies should be conducted to develop mesh pattern for $0 < H/B < 1.0$ considering normal and shear stress continuity at the interface.

2. For vertically layered soil system, the effect of the position of the strip footing, (i.e. its distance from the edge of the scope) on the bearing capacity of strip footing is to be looked at.

3. Bearing capacity of a strip footing on a weak soil adjacent to a stiffer soil, i.e. $C_1/C_2 < 1.0$ also needs to be investigated.

4. Finding lower bound solutions for braced excavations.

5. Capacity of horizontal anchors in layered soil.

6. Lower bound bearing capacity of strip footings on gravel trench embedded in soft soil.

Chapter 7

REFERENCES

Arai, K. and Tagya, K.(1985), "Limit Analysis of Geotehnical Problems by Applying Lower Bound Theorem", *Soils and foundations*, 25, No. 4, 37-48.

Basudhar, P.K. (1976), "Some Applications of Mathematical Programming Techniques to Stability Problems in Geotechnical Engineering", Ph.D. thesis, Indian Institute of Technology, Kanpur, India.

Basudhar, P.K., Madhav. M.R. and Valsangkar, A.J. (1979), "Optimal Lower Bound of Passive Earth Presure Using Finite Elements and Nonlinear Programming", *Internationl Journal for Numerical and Analytical Methods in Geomechanics*, 3, 367-379.

Basudhaar, P.K., Madhav, M.R. and Vasangkar, A.J. (1981), "Sequential Unconstrained Minimization in the Optimal Lower Bound Bearing Capacity Analysis", *Indian Geotechnical Journal*, 11, 42-55.

Basudhar, P.K. and Singh, D.N. (1993), "A Generalized Procedure for Predicting Optimal Lower Bound Breakout Factor of Strip Anchors", *Geotechnique*, 44, No. 2, 307-318.

Bottero, A., Negre, R., Pastor, J. and Turgeman, S. (1980), "Finite Element Method and Limit Analysis Theory for Soil Mechanics Problems", *Comput. Methods Appl. Mech. Engg.*, 22, 131-149.

Brown, J.D. and Meyerhof, G.G. (1969). Experimental Study of Bearing Capacity in Layered Soil. *Proceedings 7th international Conference on Soil Mechanics and Foundation Engineering*, Mexico, 2, 45-51.

Button, S.J. (1953), "The Bearing Capacity of Footing on A Two Layer Cohesive Subsoil", *Proc. 3rd Int. Conf. Soil Mech. and Fdn. Engg.*, Zurich, **1**, 332-335.

Chen, W.F. (1968), "Discussion on Applicationof Limit Plasticity in Soil Mechanics, by W.D. Lian Finn", *Journal of Soil Mech. Found. Div., ASCE*, **94, No. SM2**, 608-613.

Chen, W.F., (1969), "Discussion on Application of Limit Plasticity in Soil Mechanics, by W.D Liam Finn", *Journal of Soil Mech. Foundation., ASCE*, **95, No. SM2**, 493-518.

Chen, W.F., (1987), "Limit Analysis and Soil Plasticity", Elsevier, Amsterdam.

Chuang, P.H. (1992a), "Stability Analysis in Geotechnics by Linear Programming I : Formulation", *Journal of the Soil Mechanics and Foundations Divisions, ASCE*, **118, No. 11**, 1696-1715.

Chuang, P.H. (1992b), "Stability Analysis in Geomechanics by Linear Programming II : Application", *Journal of the Soil Mechanicsand Foundation Divisions, ASCE*, **118, No.11**, 1716-1726.

Drucker, D.C. (1953), "Limit Analysis of Two and Three dimensional Soil Mechanics Problems", *Journal of the Mechanics and Physics of Soilds*, London, **1**, 217-226.

Finn, W.D.L. (1967), "Application of Limit Plasticity in Soil Mechanics", *Journal of the Soil Mechanics and Foundation Division, ASCE*, **93, No. SM 5**, 101-120.

Flozkiewicz A. (1989), "Upper Bound to bearing capacity of Layered soils", *Canadian Geotechnical Journal*, **26**, 730-736.

Hanna, A.M. and Meyerhof, G.G. 1979,. "Ultimate Bearing Apacity of foundations on a Three Layer Soil, with Special Reference to Layered Sand", *Canadian Geotechnical Journal*, **16**, 412-414.

Lysmer, J. (1970), "Limit Analysis of Plane Problems in Soil Mechanics", *Journal of the Soil Mechanics and Foundations Division, ASCE*, **96, SM4**, 1311-1334.

Mumo, J. (1982), "Plastic Analysis in Geomechanics by Methamatical Programming", J.B. Martins (Ed.), Numerical Methods in Geomechanics, D. Reider Publishing Company, 247-272.

Radoslaw, L.M. and Lei.chi (1995), "Bearing Capacity of Footings over Two-Layer foundation Soils", *Journal of Geotechnical Engineering, ASCE*, **121(5)**, 421-428.

Reddy, A.S. and Srinivasan. R.J. (1967), "Bearing Capacity of Footings on Layered Clays", Proceedings ASCE, *Journal of Soil Mechanics and Foundations Division*, 93, No. SM2, 83-99.

Singh, D.N. (1992), "Lower Bound Solutions of Some Stability Problems in Geotechnical Engineering", Ph.D thesis, Indian Institute of Technology, Kanpur, India.

Singh, D.N. and Basudhar, P.K. (1992), "A Note on the Optimal Lower Bound Pullout Capacity of Inclined Strip Anchor in Sand", *Canadian Geotechnical Journal*, 29(5), 870-873.

Singh, D.N. and Basudhar, P.K. (1993a), "Determination of the Optimal Lower Bound Bearing Capacity of Reinforced Sol Retaining Walls by Using Finite Elements and Non-linear Programming", *Geotextiles and Geomembranes*, 12, 665-686.

Singh, D.N. and Basudhar, P.K. (1993b), "A Note on Vertical Cuts in Homogeneous Soils", *Canadian Geotechnical Journal*, 30(5), 859-863.

Singh, D.N., Basudhar, P.K. and Srivastava, S.K. (1993b), "Limit Analysis of Stability Problems in Geotechnical Engineering: State-of-the-Art", *Indian Geotechnical Journal*, 25(3), 314-342.

Sloan, S.W. (1988), "Lower Bound Limit Analysis Using Finite Elements and Linear Programming", *International Journal for Numerical and Analytical Methods in Geomechanics*, 13, 61-77.

Sloan, S.W. (1989), "Upper Bound Limit Analysis Using Finite Elements and Linear Programming", *International Journal for Numerical and Analytical Methods in Geomechanics*, 13, 263-282.

Sokolovski, V.V. (1960), "Statics of Soil Media", *Butterworth*, London

Sokolovski, V.V. (1965), "Statics of Granular Media",*Pergamon Press*, Oxford